Autophagy is required for endothelial cell alignment and atheroprotection under physiological blood flow

Anne-Clemence Vion[a,b,1], Marouane Kheloufi[a,b,c,1], Adel Hammoutene[a,b], Johanne Poisson[a,b], Juliette Lasselin[a,b], Cecile Devue[a,b], Isabelle Pic[a,b], Nicolas Dupont[b,d,e], Johanna Busse[f], Konstantin Stark[f], Julie Lafaurie-Janvore[g], Abdul I. Barakat[g], Xavier Loyer[a,b], Michele Souyri[h], Benoit Viollet[b,i,j], Pierre Julia[b,k], Alain Tedgui[a,b], Patrice Codogno[b,d,e], Chantal M. Boulanger[a,b,2,3], and Pierre-Emmanuel Rautou[a,b,c,l,2]

[a]INSERM, U970, Paris Cardiovascular Research Center, 75015 Paris, France; [b]Université Paris Descartes, Sorbonne Paris Cité, 75006 Paris, France; [c]Université Paris Diderot, Sorbonne Paris Cité, 75013 Paris, France; [d]INSERM U1151, Institut Necker-Enfants Malades-INEM, 75014 Paris, France; [e]CNRS UMR 8253, 75014 Paris, France; [f]Medizinische Klinik I, Klinikum der Universität München, 81377 Munich, Germany; [g]Mechanics & Living Systems, Cardiovascular Cellular Engineering, Laboratoire d'Hydrodynamique, Ecole Polytechnique, UMR 7646, 91128 Palaiseau, France; [h]INSERM UMR_S1131/IHU/Université Paris Diderot, 75013 Paris, France; [i]INSERM U1016, Institut Cochin, 75014 Paris, France; [j]CNRS, UMR 8104, 75014 Paris, France; [k]Service de Chirurgie Cardiaque et Vasculaire, Hôpital Européen Georges Pompidou, AP-HP, 75015 Paris, France; and [l]Département Hospitalo-Universitaire Unity, Pôle des Maladies de l'Appareil Digestif, Service d'Hépatologie, Centre de Référence des Maladies Vasculaires du Foie, Hôpital Beaujon, Assistance Publique-Hopitaux de Paris, 92110 Clichy, France

Edited by Beth Levine, The University of Texas Southwestern Medical Center, Dallas, TX, and approved August 23, 2017 (received for review February 10, 2017)

It has been known for some time that atherosclerotic lesions preferentially develop in areas exposed to low SS and are characterized by a proinflammatory, apoptotic, and senescent endothelial phenotype. Conversely, areas exposed to high SS are protected from plaque development, but the mechanisms have remained elusive. Autophagy is a protective mechanism that allows recycling of defective organelles and proteins to maintain cellular homeostasis. We aimed to understand the role of endothelial autophagy in the atheroprotective effect of high SS. Atheroprotective high SS stimulated endothelial autophagic flux in human and murine arteries. On the contrary, endothelial cells exposed to atheroprone low SS were characterized by inefficient autophagy as a result of mammalian target of rapamycin (mTOR) activation, AMPKα inhibition, and blockade of the autophagic flux. In hypercholesterolemic mice, deficiency in endothelial autophagy increased plaque burden only in the atheroresistant areas exposed to high SS; plaque size was unchanged in atheroprone areas, in which endothelial autophagy flux is already blocked. In cultured cells and in transgenic mice, deficiency in endothelial autophagy was characterized by defects in endothelial alignment with flow direction, a hallmark of endothelial cell health. This effect was associated with an increase in endothelial apoptosis and senescence in high-SS regions. Deficiency in endothelial autophagy also increased TNF-α–induced inflammation under high-SS conditions and decreased expression of the antiinflammatory factor KLF-2. Altogether, these results show that adequate endothelial autophagic flux under high SS limits atherosclerotic plaque formation by preventing endothelial apoptosis, senescence, and inflammation.

endothelial | autophagy | shear stress | atherosclerosis | inflammation

Atherosclerosis develops at arterial bifurcations and at the inner part of curvatures where blood flow is low or disturbed, whereas areas exposed to high blood flow, generating high laminar shear stress (SS) on the endothelium, remain lesion-free (1–4). Low SS is known to induce endothelial apoptosis, which in turn increases their procoagulant and proadhesive phenotype for platelets (5–7). Endothelial cells with senescence-associated phenotype are present in low-SS areas (8, 9). Senescent endothelial cells exhibit a proinflammatory phenotype that may contribute to the initiation and progression of atherosclerosis (9, 10). Low SS also stimulates endothelial expression of adhesion molecules and the release of chemokines that contribute to leukocyte recruitment, the early steps of atherosclerotic plaque formation (4, 11). However, the regulation of endothelial phenotypes by SS remains not fully elucidated.

Macroautophagy (hereafter referred to as autophagy) is a major intracellular recycling system. Under basal conditions, autophagy controls organelle and protein quality to maintain cellular homeostasis. Under conditions of stress, autophagy acts as a survival mechanism, maintaining cellular integrity by regenerating metabolic precursors and clearing subcellular debris (12). Autophagy primarily acts as a protective mechanism preventing cell death and senescence (12). This process modulates an expanding list of disease processes (12). Recent data indicate that mice deficient in endothelial Atg7, a key protein in autophagy process, develop more atherosclerotic plaques, but the mechanism remains elusive (13). Several groups have investigated the effect of SS on endothelial autophagy, with conflicting results. Most groups have found that SS activates autophagy in cultured endothelial cells (14–20), but a few investigators have compared the effects of different SS levels and reported paradoxical findings (14, 16–18, 21). The rare analyses of animal vessels did not help in drawing reliable conclusions (16, 18, 21). Importantly, the consequences of defective autophagy on endothelium health, i.e., apoptosis, senescence, and inflammatory phenotype, have not been thoroughly investigated (14). This led us to test the hypothesis that autophagy mediates the effect of SS on atherosclerosis development.

Significance

Atherosclerotic plaques tend to develop preferentially in areas of the vasculature exposed to low and disturbed shear stress (SS), but the mechanisms are not fully understood. In this study, we demonstrate that inefficient autophagy contributes to the development of atherosclerotic plaques in low-SS areas. Defective endothelial autophagy not only curbs endothelial alignment with the direction of blood flow, but also promotes an inflammatory, apoptotic, and senescent phenotype. Furthermore, genetic inactivation of endothelial autophagy in a murine model of atherosclerosis increases plaque burden exclusively in high-SS areas that are normally resistant to atherosclerotic plaque development. Altogether, these findings underline the role of endothelial autophagic flux activation by SS as an atheroprotective mechanism.

Author contributions: A.-C.V., M.K., C.M.B., and P.-E.R. designed research; A.-C.V., M.K., A.H., J.P., J.L., C.D., I.P., J.B., K.S., J.L.-J., X.L., and C.M.B. performed research; N.D., K.S., J.L.-J., A.I.B., M.S., B.V., P.J., and P.C. contributed new reagents/analytic tools; A.-C.V., M.K., X.L., A.T., P.C., C.M.B., and P.-E.R. analyzed data; and A.-C.V., M.K., A.T., P.C., C.M.B., and P.-E.R. wrote the paper.

The authors declare no conflict of interest.

This article is a PNAS Direct Submission.

[1]A.-C.V. and M.K. contributed equally to this work.

[2]C.M.B. and P.-E.R. contributed equally to this work.

[3]To whom correspondence should be addressed. Email: chantal.boulanger@inserm.fr.

This article contains supporting information online at www.pnas.org/lookup/suppl/doi:10.1073/pnas.1702223114/-/DCSupplemental.

Results

Autophagy Is Defective in Endothelial Cells Exposed to Low SS. Given the inconsistent in vitro results regarding the effect of SS on endothelial autophagy (14, 16–18, 21), we first examined endothelial autophagy level in isolated human and murine arteries by assessing LC3 punctae labeling (22). In human carotid arteries, LC3 staining was systematically less abundant in endothelial cells exposed to a disturbed low SS compared with those exposed to physiological high SS (7, 23, 24) (Fig. 1*A* and *SI Appendix*, Table S1). In murine arteries, en face LC3 staining of the inner part of the curvature of the aorta, exposed to a disturbed low SS, was significantly lower than that in the linear part of the descending thoracic aorta, exposed to a physiological high SS (Fig. 1*B*). This difference was observed in males as well as in females. Endothelial autophagy was then evaluated by measuring the LC3II/LC3I ratio in low-passage cultured human umbilical vein endothelial cells (HUVECs) exposed to 2 vs 20 dyn/cm^2 SS for as long as 24 h (Fig. 1*C*). A difference between low and high SS appeared after 12 h and was more pronounced at 24 h (Fig. 1*C*). Similar results were also observed when expressing LC3 as a ratio of LC3II to GAPDH (*SI Appendix*, Fig. S1*A*) and when measuring LC3 by flow cytometry analysis (*SI Appendix*, Fig. S1*B*). Finally, transmission EM analysis revealed a lower number of autophagic vacuoles in HUVECs exposed to low than to high SS (n = 3; Fig. 1*D*). Altogether, these results demonstrate that autophagy is reduced in endothelial cells exposed to low SS compared with high SS.

Complete autophagy requires the fusion of autophagosomes with lysosomes. To evaluate the autophagy flux, we treated HUVECs with bafilomycin A1, an inhibitor of autophagic flux. In HUVECs exposed to high SS for 6 h, bafilomycin A1 increased the LC3II/LC3I ratio, attesting to a functional autophagic flux under these conditions (Fig. 2*A*). On the contrary, bafilomycin A1 had no effect under low SS conditions, suggesting a blockade of the fusion between autophagosomes and lysosomes under these conditions (Fig. 2*A*). To confirm these data, we used a tandem monomeric red fluorescent protein (mRFP)-GFP-LC3 assay as a complementary strategy. In this assay, autophagosomes are labeled with a yellow signal (mRFP-GFP-LC3), and their maturation into autolysosomes is attested by a red signal as a result of the quenching of GFP fluorescence in lysosomes. As shown in Fig. 2*B*, RFP fluorescence was twofold lower in HUVECs exposed to low-SS compared with high-SS conditions, attesting to a blockade of autophagic flux under low SS. Similarly, colocalization of LC3 and the lysosomal marker LAMP2 was lower under low-SS than under high-SS conditions, confirming an impaired autophagic flux under low SS (Fig. 2*C*). We then investigated autophagic flux in vivo by injecting WT mice with chloroquine, an inhibitor of autophagic flux. As shown in

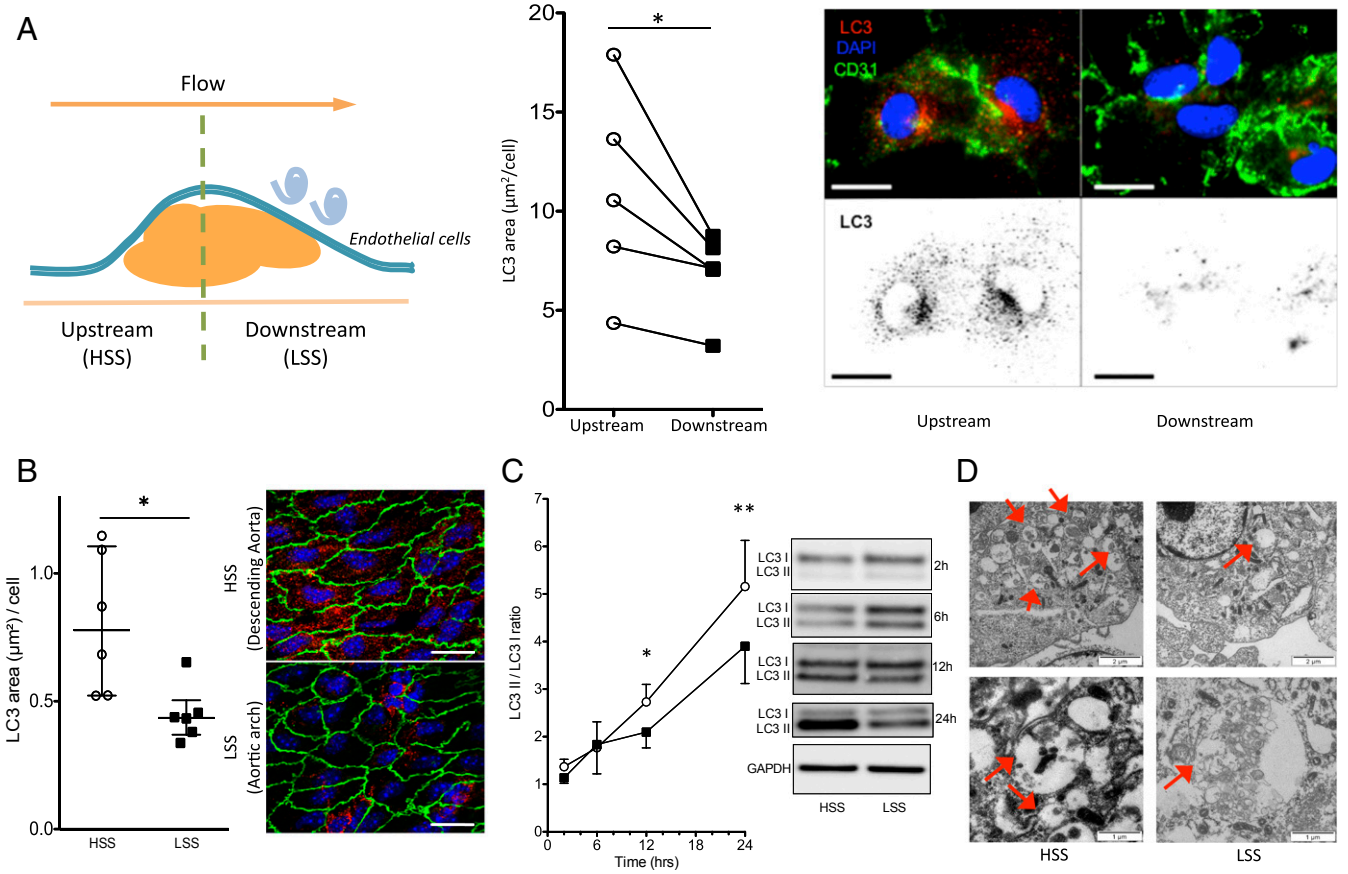

Fig. 1. Autophagy is defective in endothelial cells exposed to low SS (LSS). (*A*) LC3 en face staining of human endothelial cells isolated from endarterectomy specimen. (*Left*) Typical longitudinal section of a carotid atherosclerotic plaque showing upstream (exposed to high physiological SS) and downstream (exposed to low disturbed SS) parts. (*Middle*) Quantification. (*Right*) Representative images (green, CD31; red, LC3; blue, DAPI). (Scale bar, 10 µm.) Between 50 and 125 cells were counted per area for each patient. (*B*) LC3 en face staining of the aorta of 10-wk-old C57BL/6 mice (n = 6; green, CD31; red, LC3; blue, DAPI). (Scale bar, 20 µm). (*Left*) Quantification of LC3 area; data are given as median (horizontal bar) and interquartile range (error bar). (*Right*) Representative images. (*C*) Western blot analysis of LC3II/LC3I ratio in HUVECs exposed to high SS (HSS) and low SS. Data are normalized to static conditions for each time point ($n \geq 5$ per time point and per SS condition). Data are mean ± SEM. (*D*) Transmission EM analysis of HUVECs exposed to high and low SS for 24 h. Representative pictures of three independent experiments. Red arrows indicate autophagic vacuoles (*$P < 0.05$ and **$P < 0.01$).

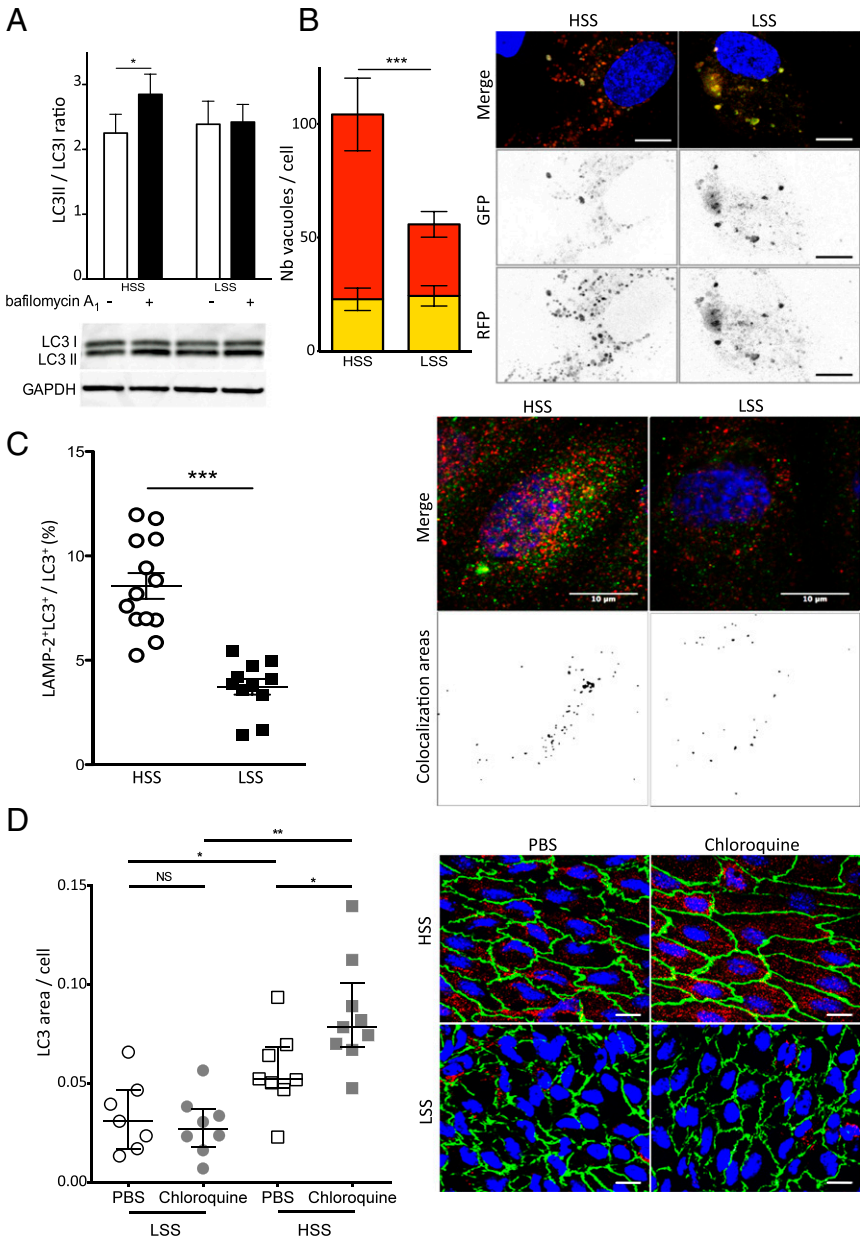

Fig. 2. Autophagic flux is blocked under low SS (LSS). (*A*) LC3 II/LC3 I ratio quantified by Western blot in HUVECs exposed to high SS (HSS) and low SS ($n = 5$; 6 h of SS including 4 h of bafilomycin A1, 100 nmol/L). (*B*) Quantification of HUVECs transfected with the tandem mRFP-GFP-LC3 plasmid and exposed for 24 h to high or low SS. Yellow bars represent autophagosomes, and red bars represent autolysosomes. Images are representative of three independent experiments in which more than 100 cells were observed. Autophagosomes are labeled with a yellow signal, whereas autolysosomes are labeled with a red signal. (Scale bar, 10 μm.) (*C*) Immunofluorescent LAMP2 and LC3 staining on HUVECs exposed to high or low SS for 24 h. (*Left*) Quantification. (*Right*) Representative images (red, LC3; green, LAMP2; blue, DAPI). Data are presented as mean ± SEM (*$P < 0.05$, **$P < 0.01$, and ***$P < 0.001$). (*D*) LC3 en face staining of the aorta of 8-wk-old C57BL/6 male mice injected i.p. with PBS solution or chloroquine (60 mg/kg/d; 48 h, 24 h, and 4 h before euthanasia; $n = 7$–9 per group; green, CD144; red, LC3; blue, DAPI). (Scale bar, 20 μm.) (*Left*) Quantification of LC3 area. Data are given as median (horizontal bar) and interquartile range (error bar). (*Right*) Representative images.

Fig. 2*D*, chloroquine enhanced LC3 staining in high-SS areas but had no effect in low-SS areas, confirming the results obtained in vitro.

We then investigated the pathways responsible for this defect in endothelial autophagy under low SS. Exposure to SS for as long as 24 h did not alter endothelial expression of the key proteins of the autophagy pathway, namely Beclin1, ATG5, and ATG7 (*SI Appendix*, Fig. S1*C* and Table S3). LAMP2 expression was also unaffected (*SI Appendix*, Fig. S1*C*). The mammalian target of rapamycin (mTOR) and AMPK pathways are master negative and positive regulators of autophagy, respectively (25). Low SS increased 4EBP1 phosphorylation, confirming the activation of mTOR pathway under these experimental conditions (26) (*SI Appendix*, Fig. S1*D*). Inhibition of mTOR by using rapamycin increased autophagy level in HUVECs exposed to low-SS condition (Fig. 3*A*). Similarly, injection of rapamycin into WT mice increased LC3 staining in endothelial cells in low-SS areas (Fig. 3*B*). As previously described, we observed reduced phosphorylation of AMPKα and of its substrate, acetyl-CoA carboxylase, under low-SS conditions (26–28) (*SI Appendix*, Fig. S1 *E* and *F*). To ascertain the implication of AMPKα in the regulation of endothelial autophagy by SS, we evaluated LC3 staining in endothelial cells from the aorta of mice deficient in *Ampkα1* (Fig. 3*C*). Endothelial LC3 staining in high-SS areas was

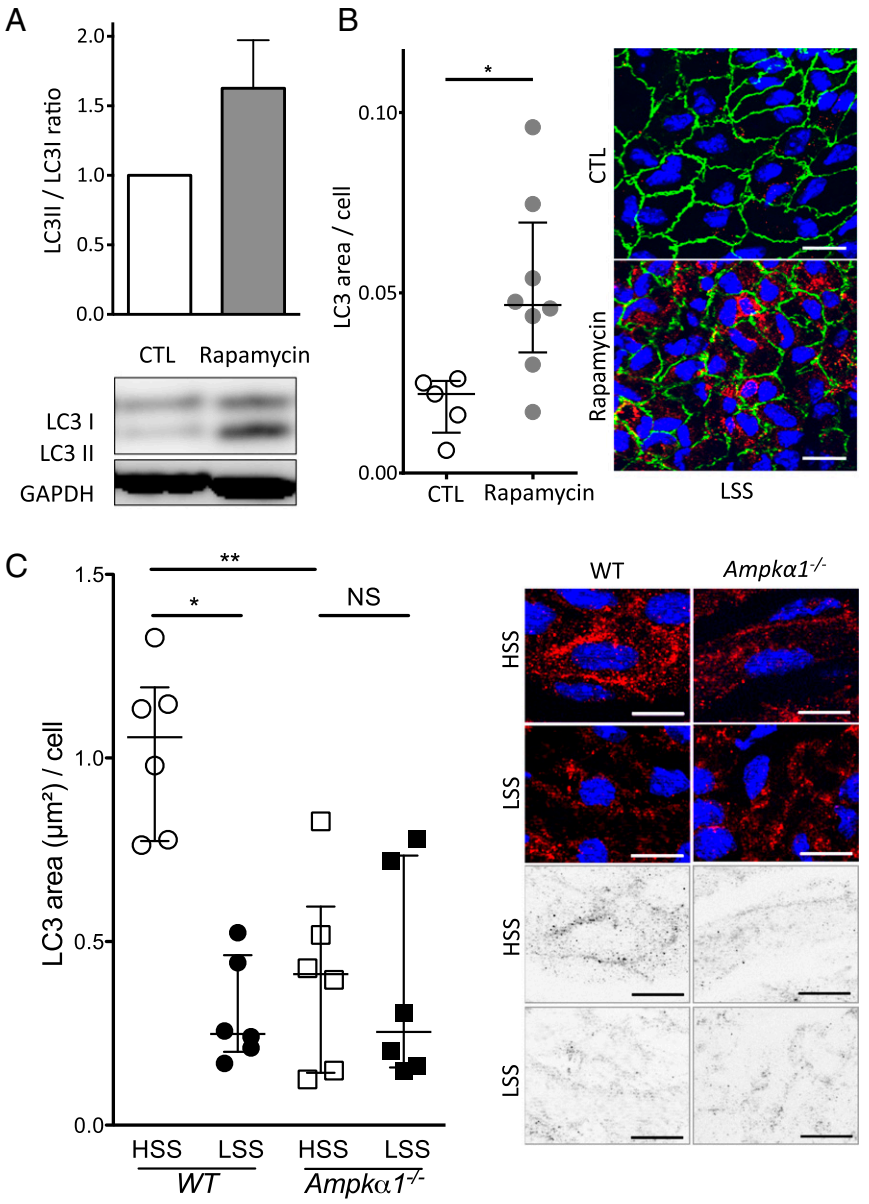

Fig. 3. Decreased AMPKα activity and increased mTOR activity concurrent with endothelial autophagy defect under low SS (LSS). (*A*) Western blot analysis of LC3II/LC3I ratio in HUVECs exposed to low SS for 24 h in the presence or absence of rapamycin (0.5 μmol/L; $n = 3$; data are normalized to static condition and are presented as mean ± SEM). (*B*) LC3 en face staining of the aorta of 9-wk-old C57BL/6 male mice injected i.p. with DMSO alone or with rapamycin (4 mg/kg/d 24 h and 4 h before euthanasia; $n = 5$ vs. $n = 8$, respectively; green, CD144; red, LC3; blue, DAPI). (Scale bar, 20 μm.) (*Left*) Quantification of LC3 area. Data are given as median (horizontal bar) and interquartile range (error bar). (*Right*) Representative images. (*C*) LC3 en face staining of the aorta of 12-wk-old *Ampkα1*-deficient and WT mice (red, LC3; blue, DAPI; $n = 6$). (Scale bar, 10 μm.) Data are given as median (horizontal bar) and interquartile range (error bar). HSS, high SS.

significantly lower in Ampkα1-deficient mice than in littermate WT mice. Moreover, endothelial LC3 labeling was not different between high- and low-SS areas of the aorta of *Ampkα1*-deficient mice, whereas it was significantly lesser in low-SS than in high-SS areas of WT mice. These results support the hypothesis that the AMPKα pathway mediates endothelial autophagy activation by high SS.

Taken together, these results demonstrate that the defect in endothelial autophagy under low-SS conditions results from an inhibition of the AMPKα and activation of the mTOR pathways and is associated with a blockade of the autophagic flux.

Atherosclerotic Lesions in Hypercholesterolemic Mice Deficient in Endothelial Autophagy. To assess the role of SS-induced autophagy on atherosclerotic plaque development, $Apoe^{-/-}$;$Atg5^{flox/flox}$; *VE-cadherin-cre* and littermate controls were fed a Western diet for 10 wk (*SI Appendix*, Fig. S2 *A* and *B*). In $Apoe^{-/-}$; $Atg5^{flox/flox}$ mice, atherosclerotic plaques formed preferentially in the curvature of the aorta, whereas the descending thoracic aorta was protected from lesion development (Fig. 4). Plaque size increased by approximately 100% in the descending thoracic aorta of mice deficient in endothelial autophagy compared with littermate controls (Fig. 4). This difference persisted even after excluding plaques at the ostia of branching arteries, which correspond to small areas of the descending thoracic aorta where SS is low (*SI Appendix*, Fig. S2*C*). Unlike the descending thoracic aorta, we observed no significant difference in plaque size in the aortic arch between the two strains (Fig. 4).

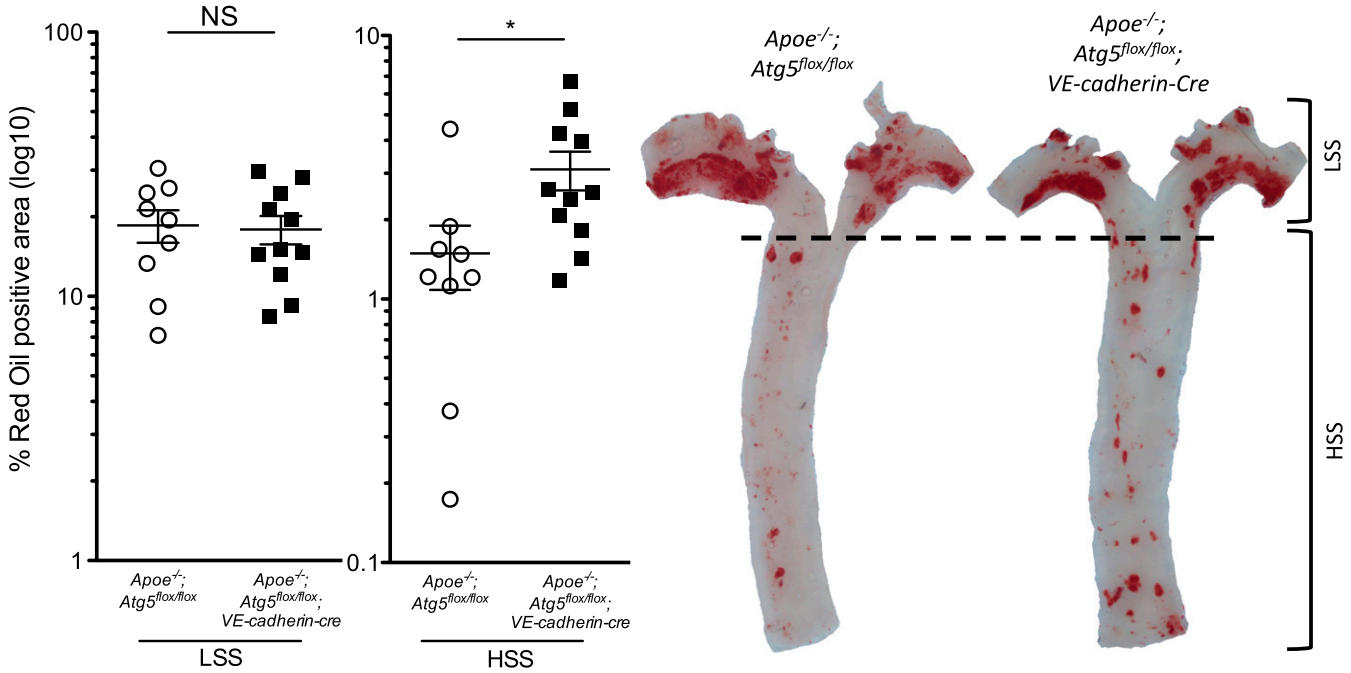

Fig. 4. Deficiency in endothelial autophagy promotes atherosclerosis. Twenty-three-week-old *Apoe*$^{-/-}$;*Atg5flox/flox* ($n = 9$) and *Apoe*$^{-/-}$;*Atg5flox/flox*;*VE-cadherin-cre* ($n = 11$) mice were fed a Western diet for 10 wk. Quantification of en face Oil Red O staining of atherosclerotic lesions in the aorta of these mice and representative images. (Scale bar, 1 mm.) Data are given as median (horizontal bar) and interquartile range (error bar; $*P < 0.05$, $**P < 0.01$, and $***P < 0.001$; HSS, high SS; LSS, low SS).

Endothelial deficiency in ATG5 in the *Apoe*$^{-/-}$ mice had no effect on arterial blood pressure and cholesterol levels, body and organ weight, or blood cell count (*SI Appendix*, Table S4). Serum glucose level was significantly higher in *Apoe*$^{-/-}$;*Atg5*$^{flox/flox}$;*VE-cadherin-cre* mice than in littermate controls, but remained in the normal range, below 126 mg/dL. These data support a direct effect of endothelial autophagy on atherosclerotic plaque formation rather than an effect on systemic metabolic parameters.

Taken together, these findings demonstrate that deficiency in endothelial autophagy promotes atherosclerotic plaque formation in atheroresistant regions.

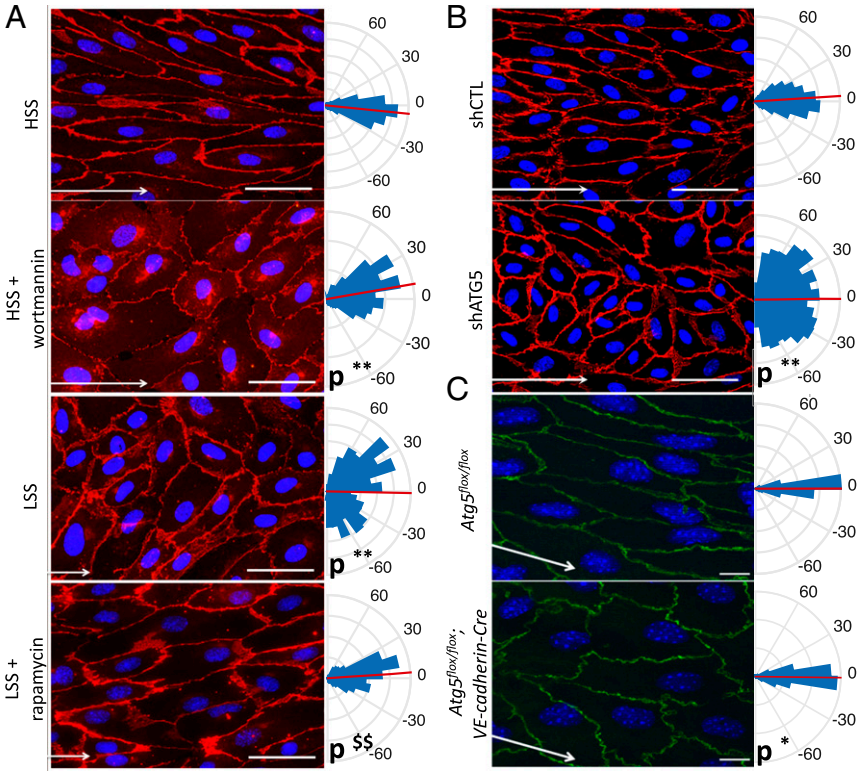

Fig. 5. Deficiency in endothelial autophagy impairs endothelial cells' ability to align in the direction of flow. (*A*) Quantification of cell alignment in the direction of flow on HUVECs treated with wortmannin [high SS (HSS)] or with rapamycin [low SS (LSS)] or not treated (red, CD144 staining; blue, DAPI; $n = 4$; more than 900 cells analyzed). (Scale bar, 50 mm.) Kuiper two-sample test: $**K_p < 0.01$ vs. WT or high-SS control, respectively; $^{\$\$}K_p < 0.01$ vs. low-SS control. White arrows represent flow direction. (*B*) Quantification of cell alignment in the direction of flow (high SS) on HUVECs infected with an shRNA control or with an shRNA targeting ATG5 ($**K_p < 0.01$). (*C*) Quantification of cell alignment in direction of flow in the linear part of the aorta (high SS) of *Atg5*$^{flox/flox}$ or *Atg5*$^{flox/flox}$;*VE-cadherin-Cre* mice (green, CD144 staining; blue, DAPI; $n = 6$; $*K_p < 0.05$). (Scale bar, 10 μm.) All panels display representative images (*Left*) and quantifications (*Right*), which are shown as rose-plot representations of endothelial axial polarity. Arcs represent cell angle with flow direction, red lines the mean of cell angle, and blue triangles the percentage of cells aligned in each direction. Each triangle represents a range of 10°.

Deficiency in Endothelial Autophagy Disturbs Endothelial Alignment in Response to Flow. The presence of lesions in areas that are normally resistant to atherosclerosis suggested a role for defective endothelial autophagy in the impairment of flow-dependent atheroprotective mechanisms. We first examined endothelial cell alignment, which is a hallmark of atheroresistant areas and plays an important role in the flow-dependent activation of antiinflammatory vs. proinflammatory pathways (3, 29, 30). We observed that HUVECs failed to align with the direction of flow under high SS when autophagy was inhibited by a pharmacological approach (i.e., wortmannin) or a genetic approach (i.e., a lentivirus expressing an ATG5 shRNA; Fig. 5 *A* and *B*). Conversely, activation of autophagy by using rapamycin in HUVECs exposed to low SS induced an alignment in flow direction (Fig. 5*A*). To investigate the relevance of these findings in vivo, we generated two models of mice deficient in endothelial autophagy, *Atg5*$^{flox/flox}$;*VE-cadherin-cre* and *Atg7*$^{flox/flox}$;*VE-cadherin-cre* mice (*SI Appendix*, Fig. S3). In these transgenic mice, deficiency in endothelial ATG5 or ATG7 had no effect on arterial blood pressure, serum glucose and cholesterol levels, or body weight, but spleen and heart weights were slightly higher in *Atg7*$^{flox/flox}$;*VE-cadherin-cre* mice but not in *Atg5*$^{flox/flox}$;*VE-cadherin-cre* (*SI Appendix*, Tables S5 and S6). In line with the observations made in vitro, endothelial alignment in the direction of flow was disturbed in high-SS areas of the aorta of mice deficient in ATG5 or ATG7 (Fig. 5*C* and *SI Appendix*, Fig. S4).

Role of PECAM-1 and of the Primary Cilium in SS Dependent Regulation of Endothelial Autophagy. One of the main flow sensors in endothelial cells is the complex formed by PECAM-1 (CD31), VE-cadherin, and VEGFR2 (31). As this complex is involved in cell orientation under flow, we evaluated its contribution to the regulation of endothelial autophagic flux. Decreasing PECAM-1 expression in HUVECs did not change the effect of high and low SS on the LC3II/LC3I ratio (*SI Appendix*, Fig. S5*A*). Similarly, LC3 en face staining of the aorta of *CD31*$^{-/-}$ mice showed the persistence of the enhanced autophagy level in high-SS areas compared with low-SS areas (*SI Appendix*, Fig. S5*B*). The primary cilium is another mechanosensor expressed by endothelial cells (32) and differentially regulated between high- and low-SS areas. Recent data indicate that the primary cilium can regulate autophagy in epithelial cells (33). To determine whether the primary cilium mediates the effect of SS on endothelial autophagy in HUVECs, we silenced KIF3a, a protein essential for primary cilium function, and exposed these cells to high and low SS. As shown in *SI Appendix*, Fig. S5*C*, the effect of SS on LC3II/LC3I ratio was not modified by the deficiency in KIF3a. Altogether, these data indicate that the mechanosensor mediating endothelial SS effect on autophagy is neither PECAM-1 nor the primary cilium.

Deficiency in Endothelial Autophagy Promotes Endothelial Inflammation. We then tested whether autophagy regulates endothelial inflammatory responses in high-SS conditions. Under control conditions, expression of KLF2 and ICAM-1 and release of MCP-1 were not different between HUVECs transduced with a lentivirus expressing an ATG5 shRNA and control cells (Fig. 6 *A*–*C*). By contrast, after exposure to the proinflammatory stimulus TNF-α, HUVECs deficient in autophagy expressed significantly less KLF2 and more ICAM-1 and released more MCP-1 than HUVECs transduced with a control shRNA (Fig. 6 *D*–*F*). This effect was not associated with an increase in autophagy level following TNF-α exposure (*SI Appendix*, Fig. S6). Altogether, these results establish that activation of endothelial autophagy by high SS is required for curbing the response to proinflammatory stimuli.

Deficiency in Endothelial Autophagy Leads to Endothelial Apoptosis. Previous in vitro data have suggested that high SS-induced autophagy could prevent apoptosis induced by H_2O_2 in endothelial cells (14). In WT mice, as expected, en face TUNEL staining showed

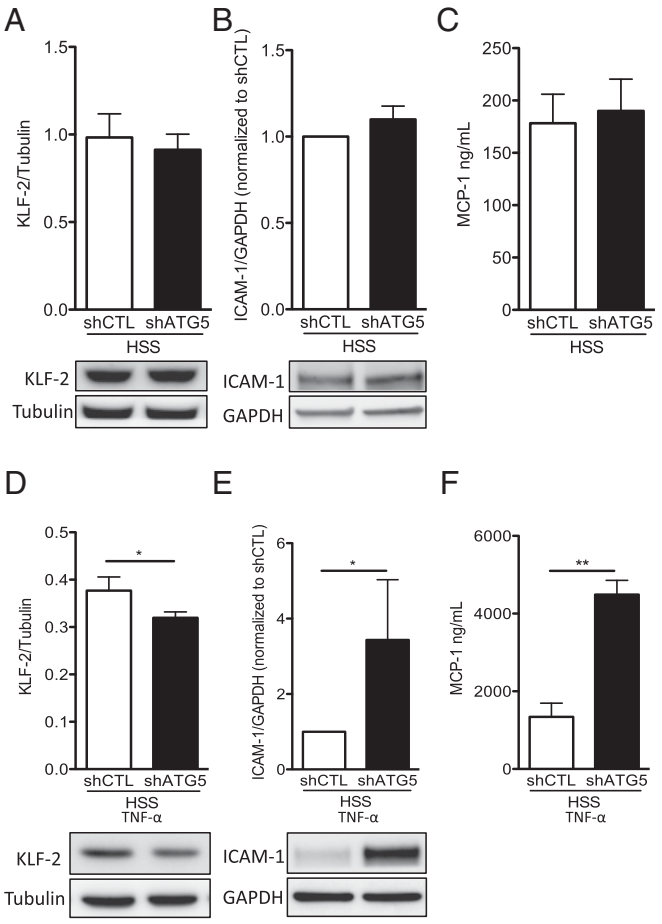

Fig. 6. Deficiency in endothelial autophagy promotes endothelial inflammation. HUVECs were transduced with a lentivirus expressing an Atg5 or a control (CTL) shRNA and exposed to high SS (HSS) for 24 h without (*A*–*C*) or with (*D*–*F*) TNF-α (1 ng/mL) for the last 12 h. (*A* and *D*) Western blot quantification of KLF-2 expression in HUVEC ($n = 6$ and $n = 5$, respectively). Data are given as mean (horizontal bar) and SEM (error bar). (*B* and *E*) Western blot quantification of ICAM-1 expression in HUVEC ($n = 4$ and $n = 6$, respectively). (*C* and *F*) Quantification of MCP1 in the supernatants of HUVECs by ELISA ($n = 8$ and $n = 6$, respectively; $^*P < 0.05$ and $^{**}P < 0.01$).

more apoptotic nuclei in endothelial cells of the inner part of the curvature of the aortic arch exposed to low SS than in those of the linear part of the aorta exposed to high SS (7) (Fig. 7*A*). Interestingly, the linear part of the aorta of mice deficient in endothelial ATG5 contained fivefold more apoptotic cells than the same area of WT mice (Fig. 7*A*). As p53 controls apoptosis, we analyzed endothelial p53 expression in vivo. We exposed 13–17-wk-old mice deficient or not in ATG5 to a high-fat diet for 5 wk as reported previously (9) (*SI Appendix*, Fig. S7*A*). We observed that mice deficient in endothelial autophagy had twice as many p53-positive nuclei in the linear part of the aorta as the controls (Fig. 7*B*). These results show that activation of endothelial autophagy by high SS prevents apoptosis.

Deficiency in Endothelial Autophagy Leads to Endothelial Senescence. As p53 also regulates senescence, we thus evaluated the role of SS-induced autophagy on endothelial senescence in cultured cells and in mice. HUVECs exposed to low SS displayed higher senescence-associated (SA)–β-gal activity than those exposed to high SS, confirming that low SS induces senescence in endothelial cells (9) (Fig. 8*A*). Pharmacological inhibition of autophagy using wortmannin under high SS increased endothelial senescence to levels similar to

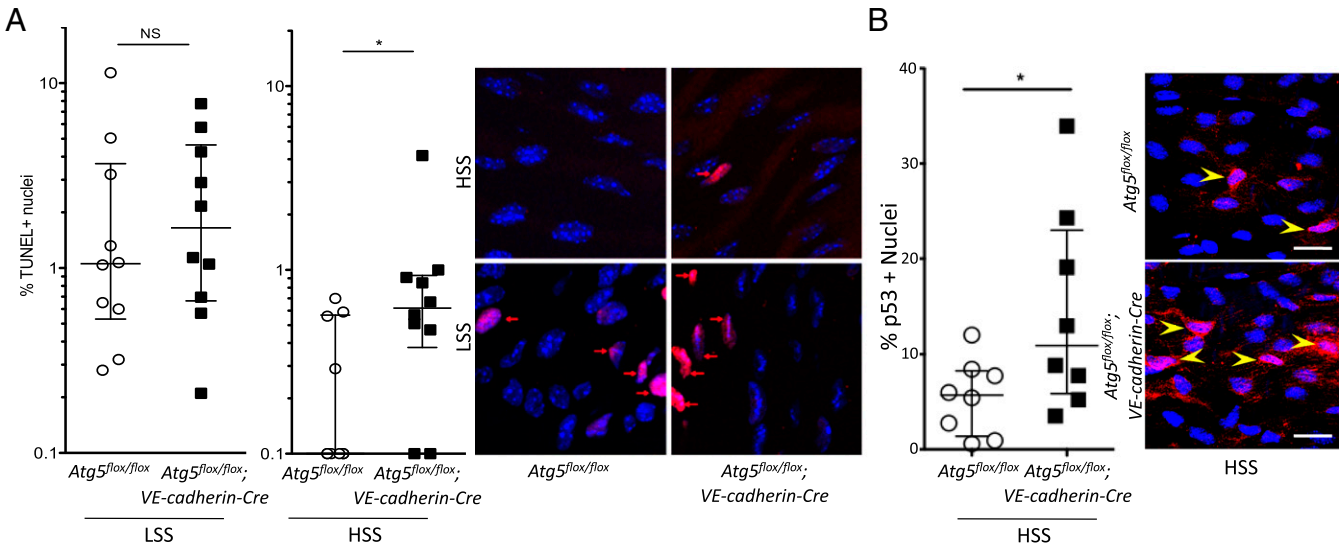

Fig. 7. Deficiency in endothelial autophagy increases apoptosis. (*A*) En face TUNEL staining of the aorta of 10-wk-old *Atg5*$^{flox/flox}$ vs. *Atg5*$^{flox/flox}$;*VE-cadherin-Cre* mice (red, TUNEL; blue, DAPI; $n = 10$). Data are given as median (horizontal bar) and interquartile range (error bar). (*B*) En face p53 staining of the descendant linear aorta [high SS (HSS)] of 13–17-wk-old *Atg5*$^{flox/flox}$ vs. *Atg5*$^{flox/flox}$;*VE-cadherin-Cre* mice fed a high-fat diet for 5 wk (red, p53; blue, DAPI; $n =$ 8 per group). (Scale bar, 20 μm.) LSS, low SS; NS, not significant (*$P < 0.05$).

those of HUVECs exposed to low-SS conditions (Fig. 8*A*). Similarly, inhibition of autophagy in HUVECs under high SS using a lentivirus expressing an ATG5 shRNA increased p16 protein expression by fourfold (Fig. 8*B*). Conversely, pharmacological activation of autophagy using rapamycin under low SS reduced senescence to a level similar to that of HUVECs exposed to high SS (Fig. 8*A*).

To assess senescence in vivo, we performed p16 en face staining on the thoracic descending part of the aorta of *Atg5*$^{flox/flox}$;*VE-cadherin-cre* vs. *Atg5*$^{flox/flox}$ mice, and observed that mice deficient in endothelial autophagy had twice as many p16-positive nuclei as the controls, attesting to a more senescent phenotype (Fig. 8*C*). To confirm these findings, we exposed 48-wk-old mice deficient in ATG5 or ATG7 and their littermate controls to a high-fat diet for 16 wk, a regimen used to better evidence endothelial senescence in vivo (34) (*SI Appendix*, Fig. S7*B*). There was no difference in serum glucose and cholesterol levels or in body and organ weight between mice deficient or not in endothelial autophagy for both models except for a slightly lower liver weight in *Atg5*$^{flox/flox}$;*VE-cadherin-cre* mice and a slightly higher heart weight in *Atg7*$^{flox/flox}$;*VE-cadherin-cre* than in littermate controls (*SI Appendix*, Tables S7 and S8). We evaluated senescence by en face SA–β-gal staining in both mouse models. As expected, in control animals, endothelial senescence was greater in the inner part of the curvature of the aortic cross, corresponding to a low-SS area, than in areas exposed to high SS (9) (Fig. 8*D* and *SI Appendix*, Fig. S7*C*). Interestingly, mice deficient in endothelial ATG5 as well as those deficient in endothelial ATG7 had 2.5 fold more senescent endothelial cells in high-SS areas of the aorta than littermate controls, whereas senescence in low-SS areas was unchanged (Fig. 8*D* and *SI Appendix*, Fig. S7*C*). Altogether, these data demonstrate that activation of endothelial autophagy by high SS protects against senescence and suggest that defective autophagy in low-SS areas is responsible for premature senescence in these regions.

Discussion

This study demonstrates that a defect in endothelial autophagy occurs in low-SS areas, impairing endothelial cell alignment in response to flow and causing endothelial inflammation, apoptosis, and senescence, thus favoring the development of atherosclerotic lesions.

The first major finding in this study was that low SS induces a defect in endothelial autophagy as a result of mTOR activation and AMPKα pathway inhibition. Conversely, high SS strongly activates autophagy. Previous analyses of the effect of various SS conditions on endothelial autophagy gave conflicting results in cultured cells (14, 16–18, 21). Fewer studies are available on blood vessels, but their results either lack sensitivity, as they were obtained with lysates from the entire arterial wall, where endothelial cells are quantitatively negligible (16, 18, 21), or used p62 immunohistochemistry, a molecule known to be regulated by SS (14, 16). Our results fill this gap in knowledge, as we observed, in human arteries, in aortas from mouse, and in cultured endothelial cells, a lower autophagy level in endothelial cells exposed to low compared with high SS. The difference in autophagic flux between the two conditions is even larger than that reflected by the LC3II/ LC3I ratio and the LC3 punctate signal we present. Indeed, under low SS, autophagic flux is blocked, leading to LC3II accumulation. Although sex differences in autophagy in various tissues have been reported in certain settings, we observed the same regulation of endothelial autophagy by SS in male and in female mice (35).

A second major finding in the present study was that a defect in endothelial autophagy enhances atherosclerotic plaque development specifically in high-SS areas where alignment of endothelial cells in the flow direction was impaired, and inflammation, apoptosis, and senescence were increased. We also tested major endothelial mechanosensors and found that neither PECAM-1, which is part of the PECAM-1/VE-cadherin/VEGFR2 complex, nor the primary cilium were implicated in signal transmission for autophagy regulation (3). The previously described endothelial dysfunction and lipid retention associated with endothelial autophagy deficiency may also contribute to atherosclerosis (13, 36). The effects we observed in the present study were not mediated by an impact on cardiovascular risk factors, as body weight, arterial blood pressure, and plasma cholesterol levels were not influenced by the deficiency in endothelial autophagy in basal conditions or under Western diet. Fasting serum glucose levels were only slightly higher in *Apoe*$^{-/-}$;*Atg5*$^{flox/flox}$;*VE-cadherin-cre* mice compared with littermate controls. However, such mild changes likely do not explain the effect we observed on atherosclerosis. Our observation that the increase in the proatherogenic phenotype and in plaque size in mice deficient in endothelial autophagy was restricted to high-SS areas implies that, under high atheroprotective SS, the autophagy level is high and prevents atherosclerosis development. Conversely, under low atherogenic SS,

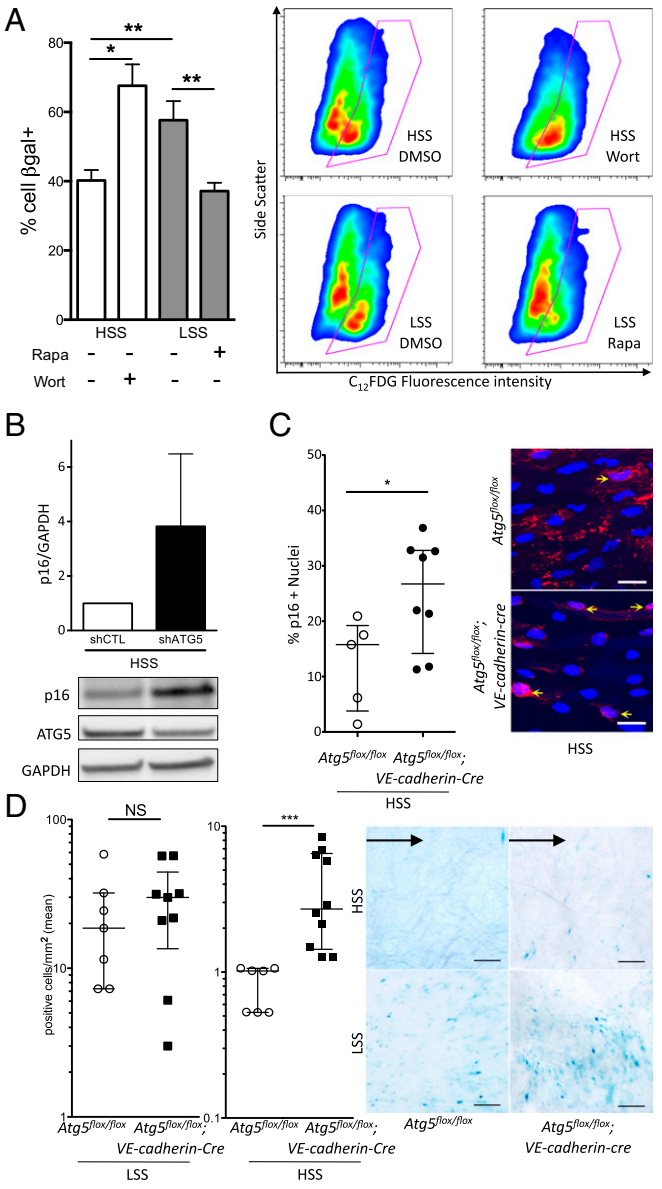

Fig. 8. Deficiency in endothelial autophagy increases senescence. (*A*) SA–β-gal activity evaluated by flow cytometry in HUVECs exposed for 24 h to high SS (HSS) with or without wortmannin (5 μmol/L) or to low SS (LSS) with or without rapamycin (0.5 μmol/L; $n \geq 6$ per condition). (*B*) Western blot analysis of p16 expression in HUVECs transduced with a lentivirus expressing an Atg5 or a control (CTL) shRNA and exposed to high SS for 24 h (shRNA induction by 1 mmol/L IPTG, $n = 5$). (*C*) En face p16 staining of the descendant linear aorta (high SS) of 48-wk-old *Atg5*$^{flox/flox}$ vs. *Atg5*$^{flox/flox}$;*VE-cadherin-Cre* mice fed a chow diet (red, p16; blue, DAPI; $n = 5$ and $n = 8$, respectively). (Scale bar, 20 μm.) (*D*) En face SA–β-gal staining of the aorta of 48-wk-old *Atg5*$^{flox/flox}$ vs. *Atg5*$^{flox/flox}$; *VE-cadherin-Cre* mice fed a high-fat diet ($n = 6$ and $n = 9$, respectively). (Scale bar, 100 μm.) Black arrow represents flow direction. The inner part of the curvature is exposed to low SS, and the descendant linear part is exposed to high SS. IPTG, isopropyl β-D-1-thiogalactopyranoside; NS, not significant (*$P < 0.05$, **$P < 0.01$, and ***$P < 0.001$).

endothelial autophagy is defective, resulting in cell death, senescence, and inflammation, which favor atherosclerosis development. The mechanisms linking SS-regulated endothelial autophagy with these various cell processes deserve further study. We can yet speculate that defective endothelial autophagy in low-SS areas induces the accumulation of damaged mitochondria, which causes increased formation of mitochondrial reactive oxygen species (37) and eventually apoptosis, senescence, and inflammation. Indeed, low or disturbed SS is known to decrease mitochondrial respiration rate and to increase mitochondrial membrane potential and superoxide anion production in endothelial cells, which can lead to endothelial apoptosis, senescence, and inflammation (11, 38, 39). Our results provide insights in the understanding of the mechanisms regulating plaque development preferentially in low- vs. high-SS areas. Our findings showing atheroprotective effects of endothelial autophagy are in line with previous studies showing that defective autophagy in vascular smooth muscle cells and macrophages promotes atherosclerosis formation and/or development (40–43). Altogether, these data indicate that inhibition of autophagy would be unfavorable as a therapeutic approach in the treatment of atherosclerosis, whereas stimulation of autophagy may be an attractive strategy.

In conclusion, low-SS atheroprone areas are characterized by low and inefficient endothelial autophagy, which triggers a defect in cell alignment as well as endothelial inflammation, apoptosis, and senescence, thereby setting the stage for the initial development of atherosclerotic lesions (Fig. 9). The defect in endothelial autophagy observed in low-SS areas may thus be the missing link between low SS and atherosclerosis development in these specific regions.

Materials and Methods

The *SI Appendix* includes further details of the study's materials and methods.

Endothelial Immunofluorescence in Human Carotid Arteries. Human atherosclerotic plaques obtained from five patients were remnants of the surgical specimens routinely processed for pathologic examination following en bloc carotid endarterectomy surgery, which was performed after patient consent (*SI Appendix*, Table S1). Institutional review board approval was not required for the human specimens at the time the work was done. The upstream part was identified from the downstream area of the lesion by using a silk thread. Endothelial cells from the upstream (i.e., high-SS) or downstream (i.e., low-SS) part of the plaque were collected separately (7, 44). Cells were fixed in 4% paraformaldehyde, permeabilized, incubated with an anti-LC3 antibody (*SI Appendix*, Table S2), and costaining with anti-CD31 antibody and DAPI.

HUVEC Culture. Confluent HUVECs (passage 2–4; 10 different primary cultures; Promocell) were cultured on 0.2% gelatin-coated slides in endothelial cell basal medium containing growth factors, 1% FCS (Promocell), streptomycin (100 IU/mL), penicillin (100 IU/mL), and amphotericin B (10 μg/L).

Plasmid Electroporation. DNA vector encoding the tandem mRFP-GFP-LC3 was used to transiently express the RFP-GFP–tagged LC3 protein to monitor the LC3 translocation and autophagosome fusion with lysosomes. In the absence of autophagy induction, the LC3 fluorescent signals are evenly distributed; upon autophagy induction, punctate fluorescent signals (i.e., yellow LC3 dots) appear as a result of LC3 accumulation on the membrane of autophagosomes; when fusion with lysosomes occurs, the punctate signal becomes red by acidic degradation of the GFP. Transfection efficacy was assessed by expression of fluorescent LC3 protein.

Lentiviral Transduction. Lentiviruses expressing inducible shRNA (Sigma-Aldrich) were used to silence Kinesin-like protein (i.e., KIF3A), ATG5, and CD31. HUVECs were infected in the presence of hexadimethrine bromide with lentiviruses. Negative controls were lentiviruses expressing a nontarget shRNA used at the same multiplicity of infection as for the protein of interest. Transduced cells were amplified and selected by using puromycin, and ShRNA expression was induced by using isopropyl β-D-1-thiogalactopyranoside.

SS Experiment in Vitro. A unidirectional steady laminar SS was applied to confluent HUVECs by using a parallel plate chamber system as described elsewhere (45). Endothelial cell medium previously filtered on a 0.1-μm membrane was perfused at different rates and for different times (1 min to 48 h). Local SS was calculated per Poiseuille's law and was 20, 2, or 0 dyn/cm^2, corresponding to high-SS, low-SS, or static conditions, respectively.

Immunofluorescent Staining and Immunofluorescence Microscopy in Vitro. To assess autophagy flux, permeabilized cells were incubated with an anti-LC3 antibody and an anti-LAMP2 antibody (*SI Appendix*, Table S2) and then with secondary antibody. For assessment of the morphology and orientation of

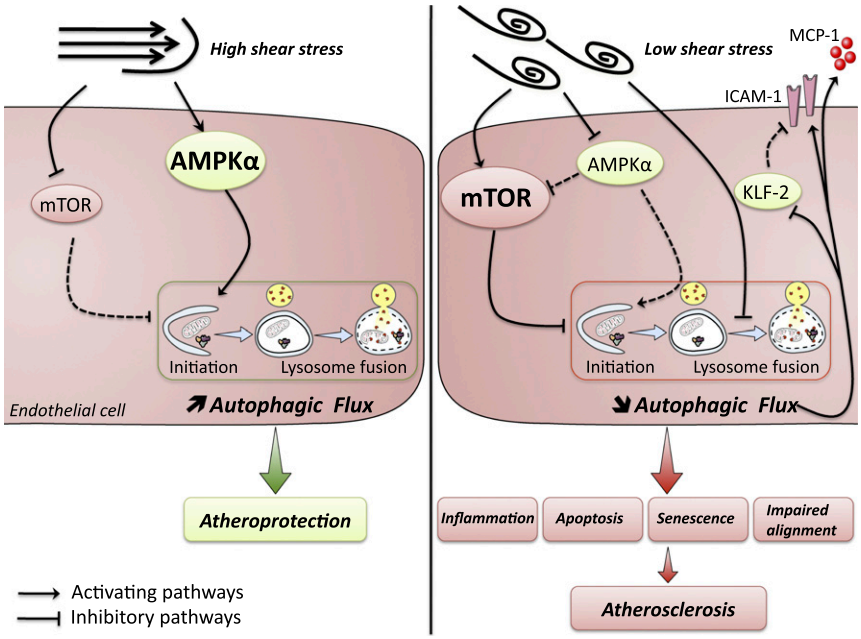

Fig. 9. Schematic illustration depicting the links between SS, autophagy, and atherosclerotic plaque formation. Under high laminar SS, endothelial autophagy is strongly induced and plays an antiapoptotic, antisenescent, antiinflammatory, and antiatherogenic role. Under low SS, a defect in endothelial autophagy occurs as a result of an inhibition of the AMPKα and activation of the mTOR pathways together with a blockade of the fusion between autophagosomes with lysosomes. This defect in endothelial autophagy leads to endothelial apoptosis, senescence, and inflammation, eventually increasing atherosclerosis development. ICAM-1, intercellular adhesion molecule 1; KLF-2, Krüppel-like factor 2; MCP-1, monocyte chemoattractant protein 1. Solid lines indicate up-regulated pathways. Dashed lines indicate down-regulated pathways.

endothelial cells under SS, HUVECs were stained with an anti-CD144 antibody. Samples were costained with DAPI to identify cell nuclei.

Transmission EM. For transmission EM experiments, the term "autophagic vesicle" refers to autophagosome or autolysosome, as it is often not possible to determine from transmission EM images whether an autophagosome has fused with a lysosome (46).

In Vitro LC3 Assessment Using Flow Cytometry. After exposure to SS, HUVECs were permeabilized by using 0.2% saponin, which specifically extracts the non–autophagosome-associated form of LC3 (47). Then, HUVECs were fixed in ethanol and incubated with an anti-LC3 antibody (47) (*SI Appendix*, Table S2). Costaining with propidium iodide for 5 min before flow-cytometry analysis was performed to identify live cells and exclude cell aggregates.

Senescence-Associated β-Gal Activity in Vitro. SA–β-gal activity was assessed by flow cytometry by using a fluorogenic substrate (C_{12}FDG; Invitrogen). After exposure to SS, HUVECs were pretreated with chloroquine diluted in medium without Phenol Red to increase the internal pH of lysosomes to 6. C_{12}FDG was then added to the medium. HUVECs were then washed and analyzed immediately. Cells not treated with C_{12}FDG were used as a negative control.

Animal Models. All mice were on a C57BL/6 background with the exception of *Ampkα1*$^{-/-}$ mice, which were on a mixed C57Bl6/129 Sv background as a result of embryonic lethality on C57Bl6 background.

Mice constitutively deficient in endothelial autophagy were obtained by crossing *VE-cadherin-Cre* transgenic mice provided by Oberlin et al. (48) with *Atg5*$^{flox/flox}$ mice provided by N. Mizushima as described by Hara et al. (49) or *Atg7*$^{flox/flox}$ mice provided by Komatsu et al. (50). Baseline morphological and metabolic features were observed, and endothelial apoptosis was assessed, in 8–17-wk-old mice fed a chow diet. For p53 experiments, 13–17-wk-old mice were fed a high fat diet for 5 wk (9). For assessment of endothelial senescence, 42–54 wk-old mice were fed the same high-fat diet for 16 wk (34). For investigation of autophagic flux in vivo, 8–9-wk-old C57BL/6 mice were injected i.p. with chloroquine (51), rapamycin (4 mg/kg/d for two consecutive days), or vehicle. To investigate the effect of endothelial autophagy on atherosclerosis development, mice constitutively deficient in endothelial autophagy (*Atg5*$^{flox/flox}$*;VE-cadherin-Cre*) were crossed with *ApoE*$^{-/-}$ mice purchased from Charles River Laboratory. Thirteen-week-old mice were fed a Western diet for 10 wk. AMPK*α1*$^{-/-}$ mice were described previously (52). *CD31*$^{-/-}$ mice were provided by Duncan et al. (53). All experiments were performed in accordance with the European Community guidelines for the care and use of laboratory animals (no. 07430) and were approved by the institutional ethical committee (no. 02526.02).

Senescence-Associated β-Gal Assay on Mouse Aortas. SA–β-gal staining was performed by incubating the aortas for 48 h at 37 °C in a CO_2-free incubator with a fresh staining solution containing 1 mg/mL X-gal. After staining, aortas were mounted en face on glass slides and imaged by using a bright-field AxioImager Z1 microscope (Zeiss).

Red-Oil Staining. Aortas were stained with a freshly prepared Oil Red O working solution, differentiated by using 70% ethanol, mounted en face, and then observed by using a bright-field microscope.

Murine Aortic Endothelial Cell Isolation. After exposure to type II collagenase, mouse aortic endothelial cells (MAECs) were collected from the aortas and seeded in a 0.1% gelatin-coated plate in DMEM supplemented with 20% FCS. MAECs were used for Western blot analysis after one passage.

En Face Immunofluorescence Microscopy on Mouse Aortas. Mouse aortas were fixed with paraformaldehyde and permeabilized by using Triton X-100. Tissues were then exposed to an anti-LC3, an anti-p53, or an anti-p16 antibody (*SI Appendix*, Table S2) and then to the respective secondary antibody. To assess apoptosis level, aortas were stained with the in situ cell death detection kit from Roche (red). In all experiments, endothelial cells were recognized by their morphology. Still, in most series of experiments, costaining with anti-CD31 antibody or anti-CD144 antibody was performed. In all mice, 8–10 images were obtained from regions in the aortic arch exposed to low SS and the thoracic aorta exposed to high SS.

Immunoblotting. HUVEC or MAEC lysates were mixed with reducing sample buffer for electrophoresis and subsequently transferred onto nitrocellulose for all blots except for p16, KLF-2, p-ACC, and ACC (PVDF membranes). Equal loading was checked by using Ponceau red solution. Membranes were incubated with primary antibodies (*SI Appendix*, Table S2). After secondary antibody incubation, immunodetection was performed by using an enhanced chemiluminescence kit [Immun-Star Western C kit (Bio-Rad) or

WesternBright Sirius (Advansta) for p16 blot], and bands were revealed by using the Las-4000 imaging system. After initial immunodetection, membranes were stripped of antibodies and reprobed with anti-GAPDH, anti-actin, or anti anti-tubulin antibodies (*SI Appendix*, Table S2).

Statistical Analysis. Data are expressed as mean ± SEM for in vitro experiments and as median (interquartile range) for in vivo experiments. Comparisons between different SS conditions or between control and treatment conditions were performed by using a Wilcoxon test. Comparisons between groups of mice were performed by using the Mann–Whitney *U* test. Comparison between sexes was performed by using a χ^2 test. Statistical analyses and figures were performed by using the SPSS statistical package software for Windows (version 20.0; SPSS) and GraphPad Prism 5 software, respectively. All tests were two-sided and used a significance level of 0.05.

Data Sharing. The data that support the findings of this study are available from the corresponding author on request.

ACKNOWLEDGMENTS. The authors acknowledge Lamia Ouchia and Marion Tanguy for their helpful contributions, Alain Grodet and Cyrielle Sophie for technical assistance in EM, the members of the INSERM U970 ERI facility, N. Mizushima for providing *Atg5*$^{flox/flox}$ mice, M. Komatsu for providing *Atg7*$^{flox/flox}$ mice, and T. W. Mak and G. Caliguiri for providing *CD31*$^{-/-}$ mice. This work was supported by the Institut National de la Santé et de la Recherche Médicale, Paris Descartes University; Fondation pour la Recherche Médicale Grant DPC20111122979; Agence Nationale pour la Recherche Grants ANR-14-CE12-0011, ANR-14-CE35-0022, and ANR-16-CE14-0015-01; Association Francaise pour l'Etude du foie Grant AFEF 2014; poste d'accueil INSERM (J.P.); Cardiovasculaire, Obésité, Diabète Domaine d'Interêt Majeur Ile de France (A.-C.V.); Ministère de la Recherche et de l'Enseignement Supérieur (M.K. and A.H.); and Fondation pour la Recherche Médicale Grant FDT20160435690 (to M.K.).

1. Chiu JJ, Chien S (2011) Effects of disturbed flow on vascular endothelium: Pathophysiological basis and clinical perspectives. *Physiol Rev* 91:327–387.
2. Gimbrone MA, Jr, García-Cardeña G (2013) Vascular endothelium, hemodynamics, and the pathobiology of atherosclerosis. *Cardiovasc Pathol* 22:9–15.
3. Hahn C, Schwartz MA (2009) Mechanotransduction in vascular physiology and atherogenesis. *Nat Rev Mol Cell Biol* 10:53–62.
4. Lusis AJ (2000) Atherosclerosis. *Nature* 407:233–241.
5. Bombeli T, Schwartz BR, Harlan JM (1999) Endothelial cells undergoing apoptosis become proadhesive for nonactivated platelets. *Blood* 93:3831–3838.
6. Dimmeler S, Haendeler J, Rippmann V, Nehls M, Zeiher AM (1996) Shear stress inhibits apoptosis of human endothelial cells. *FEBS Lett* 399:71–74.
7. Tricot O, et al. (2000) Relation between endothelial cell apoptosis and blood flow direction in human atherosclerotic plaques. *Circulation* 101:2450–2453.
8. Minamino T, et al. (2002) Endothelial cell senescence in human atherosclerosis: Role of telomere in endothelial dysfunction. *Circulation* 105:1541–1544.
9. Warboys CM, et al. (2014) Disturbed flow promotes endothelial senescence via a p53-dependent pathway. *Arterioscler Thromb Vasc Biol* 34:985–995.
10. Bai B, et al. (2012) Cyclin-dependent kinase 5-mediated hyperphosphorylation of sirtuin-1 contributes to the development of endothelial senescence and atherosclerosis. *Circulation* 126:729–740.
11. Davies PF, Civelek M, Fang Y, Fleming I (2013) The atherosusceptible endothelium: Endothelial phenotypes in complex haemodynamic shear stress regions in vivo. *Cardiovasc Res* 99:315–327.
12. Choi AM, Ryter SW, Levine B (2013) Autophagy in human health and disease. *N Engl J Med* 368:1845–1846.
13. Torisu K, et al. (2016) Intact endothelial autophagy is required to maintain vascular lipid homeostasis. *Aging Cell* 15:187–191.
14. Liu J, et al. (2015) Shear stress regulates endothelial cell autophagy via redox regulation and Sirt1 expression. *Cell Death Dis* 6:e1827.
15. Lien SC, et al. (2013) Mechanical regulation of cancer cell apoptosis and autophagy: Roles of bone morphogenetic protein receptor, Smad1/5, and p38 MAPK. *Biochim Biophys Acta* 1833:3124–3133.
16. Li R, et al. (2015) Disturbed flow induces autophagy, but impairs autophagic flux to perturb mitochondrial homeostasis. *Antioxid Redox Signal* 23:1207–1219.
17. Guo F, et al. (2014) Autophagy regulates vascular endothelial cell eNOS and ET-1 expression induced by laminar shear stress in an ex vivo perfused system. *Ann Biomed Eng* 42:1978–1988.
18. Ding Z, et al. (2015) Hemodynamic shear stress modulates endothelial cell autophagy: Role of LOX-1. *Int J Cardiol* 184:86–95.
19. Bharath LP, et al. (2014) Impairment of autophagy in endothelial cells prevents shear-stress-induced increases in nitric oxide bioavailability. *Can J Physiol Pharmacol* 92: 605–612.
20. Yao P, Zhao H, Mo W, He P (2016) Laminar shear stress promotes vascular endothelial cell autophagy through upregulation with Rab4. *DNA Cell Biol* 35:118–123.
21. Hashem SI, et al. (2015) Brief report: Oxidative stress mediates cardiomyocyte apoptosis in a human model of Danon disease and heart failure. *Stem Cells* 33:2343–2350.
22. Klionsky DJ, et al. (2016) Guidelines for the use and interpretation of assays for monitoring autophagy (3rd edition). *Autophagy* 12:1–222, and erratum (2016) 12: 443.
23. Ku DN, Giddens DP, Zarins CK, Glagov S (1985) Pulsatile flow and atherosclerosis in the human carotid bifurcation. Positive correlation between plaque location and low oscillating shear stress. *Arteriosclerosis* 5:293–302.
24. Zarins CK, et al. (1983) Carotid bifurcation atherosclerosis. Quantitative correlation of plaque localization with flow velocity profiles and wall shear stress. *Circ Res* 53: 502–514.
25. Gatica D, Chiong M, Lavandero S, Klionsky DJ (2015) Molecular mechanisms of autophagy in the cardiovascular system. *Circ Res* 116:456–467.
26. Guo D, Chien S, Shyy JY (2007) Regulation of endothelial cell cycle by laminar versus oscillatory flow: Distinct modes of interactions of AMP-activated protein kinase and Akt pathways. *Circ Res* 100:564–571.
27. Zhang Y, et al. (2006) AMP-activated protein kinase is involved in endothelial NO synthase activation in response to shear stress. *Arterioscler Thromb Vasc Biol* 26: 1281–1287.
28. Kröller-Schön S, et al. (2012) α1AMP-activated protein kinase mediates vascular protective effects of exercise. *Arterioscler Thromb Vasc Biol* 32:1632–1641.
29. Chien S (2007) Mechanotransduction and endothelial cell homeostasis: The wisdom of the cell. *Am J Physiol Heart Circ Physiol* 292:H1209–H1224.
30. Wang C, Baker BM, Chen CS, Schwartz MA (2013) Endothelial cell sensing of flow direction. *Arterioscler Thromb Vasc Biol* 33:2130–2136.
31. Tzima E, et al. (2005) A mechanosensory complex that mediates the endothelial cell response to fluid shear stress. *Nature* 437:426–431.
32. Egorova AD, van der Heiden K, Poelmann RE, Hierck BP (2012) Primary cilia as biomechanical sensors in regulating endothelial function. *Differentiation* 83:S56–S61.
33. Orhon I, Dupont N, Pampliega O, Cuervo AM, Codogno P (2015) Autophagy and regulation of cilia function and assembly. *Cell Death Differ* 22:389–397.
34. Wang CY, et al. (2009) Obesity increases vascular senescence and susceptibility to ischemic injury through chronic activation of Akt and mTOR. *Sci Signal* 2:ra11.
35. Gottlieb RA, Andres AM, Sin J, Taylor DP (2015) Untangling autophagy measurements: All fluxed up. *Circ Res* 116:504–514.
36. LaRocca TJ, et al. (2012) Translational evidence that impaired autophagy contributes to arterial ageing. *J Physiol* 590:3305–3316.
37. Mai S, Muster B, Bereiter-Hahn J, Jendrach M (2012) Autophagy proteins LC3B, ATG5 and ATG12 participate in quality control after mitochondrial damage and influence lifespan. *Autophagy* 8:47–62.
38. Bretón-Romero R, et al. (2014) Laminar shear stress regulates mitochondrial dynamics, bioenergetics responses and PRX3 activation in endothelial cells. *Biochim Biophys Acta* 1843:2403–2413.
39. Paneni F, Diaz Cañestro C, Libby P, Lüscher TF, Camici GG (2017) The aging cardiovascular system: Understanding it at the cellular and clinical levels. *J Am Coll Cardiol* 69:1952–1967.
40. Grootaert MO, et al. (2015) Defective autophagy in vascular smooth muscle cells accelerates senescence and promotes neointima formation and atherogenesis. *Autophagy* 11:2014–2032.
41. De Meyer GR, et al. (2015) Autophagy in vascular disease. *Circ Res* 116:468–479.
42. Razani B, et al. (2012) Autophagy links inflammasomes to atherosclerotic progression. *Cell Metab* 15:534–544.
43. Liao X, et al. (2012) Macrophage autophagy plays a protective role in advanced atherosclerosis. *Cell Metab* 15:545–553.
44. Choi G, et al. (2015) Coronary artery axial plaque stress and its relationship with lesion geometry: Application of computational fluid dynamics to coronary CT angiography. *JACC Cardiovasc Imaging* 8:1156–1166.
45. Ramkhelawon B, et al. (2009) Shear stress regulates angiotensin type 1 receptor expression in endothelial cells. *Circ Res* 105:869–875.
46. Eskelinen EL (2005) Maturation of autophagic vacuoles in mammalian cells. *Autophagy* 1:1–10.
47. Eng KE, Panas MD, Karlsson Hedestam GB, McInerney GM (2010) A novel quantitative flow cytometry-based assay for autophagy. *Autophagy* 6:634–641.
48. Oberlin E, et al. (2010) VE-cadherin expression allows identification of a new class of hematopoietic stem cells within human embryonic liver. *Blood* 116:4444–4455.
49. Hara T, et al. (2006) Suppression of basal autophagy in neural cells causes neurodegenerative disease in mice. *Nature* 441:885–889.
50. Komatsu M, et al. (2005) Impairment of starvation-induced and constitutive autophagy in Atg7-deficient mice. *J Cell Biol* 169:425–434.
51. Orhon I, et al. (2016) Primary-cilium-dependent autophagy controls epithelial cell volume in response to fluid flow. *Nat Cell Biol* 18:657–667.
52. Jørgensen SB, et al. (2004) Knockout of the alpha2 but not alpha1 5′-AMP-activated protein kinase isoform abolishes 5-aminoimidazole-4-carboxamide-1-beta-4-ribofuranosidebut not contraction-induced glucose uptake in skeletal muscle. *J Biol Chem* 279:1070–1079.
53. Duncan GS, et al. (1999) Genetic evidence for functional redundancy of platelet/endothelial cell adhesion molecule-1 (PECAM-1): CD31-deficient mice reveal PECAM-1-dependent and PECAM-1-independent functions. *J Immunol* 162:3022–3030.

Materials and methods

Endothelial immunofluorescence in human carotid arteries.

Human atherosclerotic plaques obtained from 5 patients were remnants of the surgical specimen routinely processed for pathology following *en bloc* carotid endarterectomy surgery performed after patient consent. Institutional Review Board approval was not required for the specimens at the time the work was done. The surgeon identified the upstreaming from the downstream area of the lesion using a silk threat. The clinical features of these patients are presented in SI Appendix, Table S1. The plaques were immediately scraped off in order to isolate endothelial cells. The upstream part of the plaque was defined as the area between the beginning of the plaque and the site of maximal stenosis. The downstream part was defined as the area between the site of maximal stenosis and the end of the plaque. Endothelial cells coming from the upstream (high SS) or the downstream (low SS) part of the plaque were collected separately (1,2). Plaques were included in this study when upstream and downstream parts were clearly visible and occlusion was absent. We did not include plaques with erosion or rupture because we could not determine whether the rupture occurred *in vivo* or during the surgical manipulation of the specimen. Endothelial cells were then pulled down on a slide using a cytospin centrifuge (Cytospin™ 4 Cytocentrifuge, Thermo scientific), fixed in 4% paraformaldehyde and permabilized (0.01% triton-X100). Cells were incubated with an anti-LC3 antibody (SI Appendix, Table S2) and then with secondary antibody (anti-rabbit AlexaFluor594, Life technologies). Co-staining with anti-CD31 antibody (using a secondary anti-goat AlexaFluor488 antibody, Life technologies) was performed to identify endothelial cells. Cells were then co-stained with DAPI (0.1 µg/mL, Sigma) in order to identify cell nuclei. Samples were analyzed using a Zeiss Axio Imager Z1 fluorescence microscope equipped with a Zeiss ApoTome system (Zeiss).

Human Umbilical Vein Endothelial Cell culture.

Confluent Human Umbilical Vein Endothelial cells (HUVEC; passage 2 to 4; 10 different primary cultures were used; Promocell, Heidelberg, Germany) were cultured on 0.2 %

gelatin-coated slides (Menzel Glazer; Braunschweig, Germany) in endothelial cell basal medium containing growth factors, 1 % fetal calf serum (Promocell), streptomycin (100 IU/mL), penicillin (100 IU/mL) and Amphotericin B (10 μg/L) (Gibco).

Plasmid electroporation.

DNA vector encoding the tandem mRFP-GFP-LC3 was used to transiently express the RFP-GFP tagged LC3 protein, in order to monitor the LC3 translocation and autophagosomes fusion with lysosomes. In the absence of autophagy induction, the LC3 fluorescent signals are evenly distributed; upon autophagy induction, punctate fluorescent signals (yellow LC3 dots) appear as a result of LC3 accumulation on the membrane of autophagosomes; when fusion with lysosomes occurs, the punctate signal becomes red by acidic degradation of the GFP. Cells were used at 50 to 60% confluence for cDNA transfection by use of Nucleofector (Lonza/Amaxa) according to the manufacturer's instructions. Briefly, 5×10^6 HUVECs were electroporated with 2 μg of plasmid, using the U-01 program, and then replated in endothelial cell basal medium containing 1% fetal calf serum for 6h. The medium was then changed and cells reached confluence within 48 hours. Transfection efficacy was assessed by expression of fluorescent LC3 protein.

Lentiviral transduction.

Lentiviruses expressing inducible shRNA (Sigma Aldrich) were used to silence Kinesin-like protein (KIF3A), ATG5 and CD31. HUVECs were infected in the presence of hexadimethrine bromide (at 8 μg/mL) with lentiviruses at multiplicity of infection (MOI) 2.5 for KIF3a and ATG5 or MOI 5 for CD31. Negative controls were lentiviruses expressing a non-target shRNA used at the same MOI as for the protein of interest. Transduced cells were amplified and selected using puromycine (Sigma Aldrich #P9620) at 1 μg/mL during amplification and experiments. ShRNA expression was induced by treating HUVECs for 10 days using Isopropyl β-D-1-thiogalactopyranoside (IPTG, Sigma Aldrich; #I6758) at 1 mmol/L for KIF3A, 0.1 mmol/L for CD31 and 5 days at 1 mmol/L for ATG5.

Shear stress experiment in vitro.

A unidirectional steady laminar SS was applied to confluent HUVECs using a parallel plate chamber system as described elsewhere (3). Endothelial cell medium previously filtered on a 0.1 μm membrane was perfused at different rates and for different times (1 min to 48 hours). Local SS was calculated using Poiseuille's law and was 20, 2 or 0 dynes/cm^2, corresponding to high, low SS or static conditions, respectively.

In some experiments, cells were treated with Bafilomycin A1 (Vacuolar-type H+ -ATPase inhibitor, 100 nmol/L) for 2 hours before ending the SS experiment in order to assess autophagic flux, or with rapamycin (0.5 µmol/L, Sigma) or wortmannin (5 µmol/L, Sigma) in order to modulate autophagy level. For inflammation experiments, cells were treated with TNFα (1 ng/mL) 12 hours before the end of the flow experiment. In control conditions, HUVECs were incubated with the same concentration of the solvent (DMSO). Cells were then collected for Western blot, immunofluorescent microscopy or transmission electron microscopy, as detailed below. For ELISA, the supernatant were collected after the SS experiment, centrifuged for 15 minutes at 600g in order to remove cell debris and stored at -80°C until analysis.

Immunofluorescent staining and Immunofluorescence microscopy in vitro.

After SS exposure, HUVECs were fixed with 4% PFA and permeabilized using 0.1% Triton X-100 and blocked with 5% bovine serum albumin for 1 hour. To assess autophagy flux, cells were incubated with an anti-LC3 antibody and an anti-LAMP2 antibody (SI Appendix, Table S2) and then with secondary antibody (anti-rabbit AlexaFluor594 or anti-goat AlexaFuor 488 respectively, Life technologies). Autophagic flux was also assessed using cells transfected with the tandem mRFP-GFP-LC3 plasmid and exposed to SS. Images were acquired using a Leica SP5 confocal microscope (Leica).

For assessment of the morphology and orientation of endothelial cells under shear stress, HUVECs were stained with an anti-CD144 antibody (SI Appendix, Table S2) and a

secondary anti-goat AlexaFluor594 antibody (Life technologies). Samples were analyzed using a Zeiss Axio Imager Z1 fluorescence microscope equipped with a Zeiss ApoTome system (Zeiss).

For all the immunofluorescence experiments, samples were costained with DAPI (0.1 µg/mL, Sigma) in order to identify cell nuclei.

Transmission electron microscopy (TEM).

Transmission electron microscopy observations were performed at the IFR83-Jussieu-Paris core facility. Briefly, HUVECs were fixed with Karnovsky's fixative adapted for vascular tissues and cells (2% paraformaldehyde, 2.5% glutaraldehyde and 0.1 mol/L sodium phosphate buffer, Electron Microscopy Sciences, Hatfield, PA). After dehydration in ethanol, cells were embedded in Epon. Grids were analyzed with a transmission electron microscope (EM 912 OMEGA, ZEISS) equipped with a LaB6 filament at 80 kV. Images were captured with a digital camera (SS-CCD, Proscan 1kx1k) and with custom software.

For morphometric analysis, a minimum of 10 random fields per condition and per experiment were taken in a blinded manner at a magnification of 23,200x (>450 µm² per condition and per experiment). Electron microscopy findings were then assessed by 3 readers (ACV, PER and AH) unaware of SS condition. For TEM experiments, the term autophagic vesicle refers to autophagosome or autolysosome since it is often not possible to determine from TEM images whether or not an autophagosome has fused with a lysosome (4).

In vitro LC3 assessment using flow cytometry.

After exposure to SS, HUVECs were permeabilized using 0.2% saponin for 10 minutes and then washed 3 times with phosphate buffered saline (PBS). Saponin specifically extracts the nonautophagosome-associated form of LC3 (5). Then, HUVECs were fixed in 95% ethanol and incubated with an anti-LC3 antibody (SI Appendix, Table S2) and with an anti-rabbit anti-rabbit AlexaFluor488 antibody as described (5). Costaining with propidium iodide for 5 min prior to flow cytometry analysis was performed to identify live cells and exclude cell

aggregates. HUVECs were analyzed using a LSRII flow cytometer (BD Biosciences), and results were expressed as mean fluorescent intensity among live cells.

Senescence-associated beta-galactosidase activity in vitro.

SA-β-galactosidase activity was assessed by flow cytometry using a fluorogenic substrate (C_{12}FDG, Invitrogen). After exposure to SS, HUVECs were pretreated with chloroquine (300 µmol/L, Sigma) diluted in endothelial cell medium without phenol red for 1 hr in order to increase the internal pH of lysosomes to 6. C_{12}FDG (33 µmol/L) was then added to the medium for 1 hr. HUVECs were then washed with PBS at 4°C, resuspended and analyzed immediately using a LSR FortessaTM flow cytometer (BD Biosciences). Light scatter parameters were used to exclude dead cells and subcellular debris. The C_{12}-fluorescein signal was acquired using the FL1 detector. Data were analyzed using FlowJo software to determine the percentage of SA-β-gal positive cells. Cells not treated with C_{12}FDG were used as a negative control.

Animal models.

All mice were on a C57BL/6 background with the exception of *Ampkα1 -/-* mice, which were on a mixed C57Bl6/129 Sv background due to embryonic letality on C57Bl6 background.

Mice constitutively deficient in endothelial autophagy were obtained by crossing *VE-cadherin-Cre* transgenic mice provided by M. Souyri (6), with *Atg5*$^{flox/flox}$ mice provided by N. Mizushima (7) or *Atg7*$^{flox/flox}$ mice were provided by M. Komatsu (8). For characterization of baseline morphological and metabolic features and assessment of endothelial apoptosis, mice were fed a chow diet and were euthanized between 8 and 17 weeks of age. For assessment of endothelial p53 expression, 13 to 17 week old mice were fed a high fat diet (D12492, 26.2% protein, 26.3% carbohydrate, 34.9% fat weight to weight, Research Diets) for 5 weeks and were euthanized (9). For assessment of endothelial senescence, 42 to 54 week old mice were fed the same high fat diet for 16 weeks and were euthanized (10).

To investigate the effect of endothelial autophagy on atherosclerosis development, mice constitutively deficient in endothelial autophagy (*Atg5$^{flox/flox}$;VE-cadherin-Cre*) were crossed with *ApoE$^{-/-}$* mice purchased from the Charles Rivers laboratory. 13 week-old mice were fed a western diet (D12079B, 20% protein, 50% carbohydrate, 21% fat weight to weight, Research Diets) for 10 weeks and were then euthanized. AMPKα*1-/-* mice were described previously (11). *CD31-/-* mice were provided by T.W. Mak (12). All experiments were performed in accordance with the European Community guidelines for the care and use of laboratory animals (N°07430) and were approved by our institutional ethical committee (02526.02).

For investigation of autophagic flux *in vivo*, 8 to 9 weeks old C57BL/6 mice were injected intraperitoneally with chloroquine (60 mg/kg/day for 3 consecutive days, as described previously (13)) or rapamycin (4 mg/kg/day for 2 consecutive days) or with the corresponding vehicle.

Blood pressure measurement.

Arterial blood pressure was measured every 30 seconds at the tail of conscious mice using a CODA non-invasive blood pressure device (Kent Scientific Corporation) (mean value of 15 measurements). Blood pressure was measured for 3 consecutive days after 2 days of acclimation in the chamber.

Fasting plasma glucose and cholesterol levels.

Three days before sacrifice, mice were fasted for 6 hours. For blood glucose analysis, the distal 1 mm of the tail was excised using sterile scissors. The first blood drop was discarded; then serum glucose level was determined using OneTouch Ultra® reactive strips and OneTouch Ultra® reader (Lifescan). For plasma cholesterol analysis, mice were anesthetized with 2% isoflurane. Then, 75 μL of blood were collected from the peri-orbital venous sinus using a heparinized microhematocrit tube (Hirschmann-Laborgeräte). Blood was then centrifuged twice at 2,500 g for 15 min at room temperature to prepare platelet free

plasma and stored at -80°C until analysis. Plasma cholesterol level was determined using the Cholesterol RTU™ commercial kit (BioMérieux).

Plasma preparation.

On the day of sacrifice, non-fasted mice were sedated with 2% isofluorane. Blood was collected from the inferior vena cava using a 25 gauge x 1' needle in a 1 mL syringe pre-coated with 3.8% sodium citrate. The mice were then humanely euthanized. Blood was centrifuged at 1,500 g for 15 minutes at 18°C in order to pellet cells. Then, plasma was centrifuged at 13,000 g for 5 minutes at 18°C to pellet platelets and cell debris. Platelet free plasma (PFP) was aliquoted and stored at -80°C for measurement of circulating levels of inflammatory molecules.

Senescence-associated beta-galactosidase assay on mouse aortas.

Mouse aortas were collected fresh, micro-dissected under a Nikon SMZ 745 dissecting microscope to remove extra fat and fixed for 8 min in 2% formaldehyde and 0.2% glutaraldehyde in PBS. Beta-galactosidase staining was performed by incubating the aortas for 48 hours at 37°C in a CO_2-free incubator with a fresh staining solution containing 1 mg/mL X-gal, 0.2 mol/L citric acid/sodium phosphate, 5 mmol/L potassium ferrocyanide, 5 mmol/L potassium ferricyanide, 150 mmol/L NaCl and 2 mmol/L $MgCl_2$ at pH 6.0. After staining, aortas were washed with PBS, mounted "*en face*" on glass slides and imaged using a bright field Zeiss Axio Imager Z1 (Zeiss) microscope. Images were acquired at 100 X magnification and the number of SA-β-gal positive cells/μm^2 was quantified by two independent operators (MK and JP) unaware of mice genotype.

Red-oil staining.

Mouse aortas were first injected with PBS then with PBS supplemented with 4% paraformaldehyde, dissected and kept in PBS supplemented with 4% paraformaldehyde for 2 hours. Then, aortas were stained with a freshly prepared Oil Red O working solution (40%

distilled water, 60% of a 5 g/L Oil Red O in isopropanol; Sigma) for 30 minutes under agitation. Aortas were then differentiated using 70% ethanol for 5 minutes, mounted "*en face*" on glass slides and then observed using a bright field microscope (Leica M165FC, camera 425). Plaque size was quantified using the ImageJ software.

Murine aortic endothelial cell isolation.

The mouse vasculature was rinsed by injecting *in situ* 10 mL of Dulbecco's modified Eagle's medium (DMEM) (Gibco) into the left ventricle. Aortas were then retrieved, injected with 1 mg/mL type II Collagenase (Worthington) using a BD Insyte™ Autoguard™ catheter (BD) and incubated at 37°C for 45 minutes. Mouse aortic endothelial cells (MAEC) were collected by flushing the aortas with 10 mL DMEM, and then pelleted by centrifugation at 1000 g for 7 min before being seeded in a 0.1% gelatin-coated 12 well plate in DMEM supplemented with 20 % fetal calf serum (Gibco). After 24 hours, the medium was changed to Endothelial cell growth medium MV with growth factors (Promocell) and 5% fetal calf serum. By flow cytometry, we observed that 92% and 62% of the MAECs were positive for the endothelial markers CD-31 and eNOS, respectively and 0% were positive for smooth muscle cell and fibroblast markers (α-SMC-actin and ER-TR7, respectively). MAECs were used for Western blot analysis after one passage.

***En face* immunofluorescence microscopy on mouse aortas.**

Mouse aortas were injected *in situ* with PBS supplemented with 4% paraformaldehyde. After dissection, the tissues were permeabilized using 0.2% Triton X-100 and blocked with 5% bovine serum albumin for 20 minutes. To assess autophagy level, aortas were first incubated with an anti-LC3 antibody (SI Appendix, Table S2) and then with secondary antibody (anti-rabbit AlexaFluor594, Life technologies). To assess p53 and p16 localization, aortas were first incubated with an anti-p53 or an anti-p16 antibody (SI Appendix, Table S2) and then with secondary antibody (anti-mouse AlexaFluor594, Thermo Scientific, respectively). To assess apoptosis level, aortas were stained with the *in situ* cell death detection kit from Roche (red,

Neuilly-sur-Seine, France) according to manufacturer's instructions. In all experiments, endothelial cells were easily recognized by their morphology. Still, in most series of experiment, a co-staining with anti-CD31 antibody (using a secondary anti-goat AlexaFluor488 antibody, Life technologies) or anti-CD144 antibody (Santa Cruz biotechnology sc-6458) was performed. In all mice, 8 to 10 images were obtained from regions in the aortic arch exposed to low SS and the thoracic aorta exposed to high SS. For all these immunofluorescence experiments samples were co-stained with DAPI (0.1 µg/mL, Sigma) in order to identify cell nuclei. Samples were analyzed using a Zeiss Axio Imager Z1 fluorescence microscope equipped with a Zeiss ApoTome system (Zeiss).

ELISA.

Levels of MCP-1 in surpernatant of HUVECs were assessed by an ELISA assay (R&D, human MCP-1 Duo-set DY279) following the manufacturer's instructions.

Immunoblotting.

HUVECs or MAECs were washed with cold PBS and scraped off in RIPA buffer (150 mmol/L NaCl, 50 mmol/L TrisHCl, pH 7.4, 2 mmol/L EDTA, 0.5% sodium deoxycholate, 0.2% sodium dodecyl sulfate, 2 mmol/L activated orthovanadate, complete protease inhibitor cocktail tablet (Complet mini, Roche, France) and complete phosphatase inhibitor cocktail tablet (Roche, France)). Lysates were sonicated (15 seconds, 40 watts, Vibra Cell, Bioblock), and protein content was quantified using the Lowry protein assay (Bio-Rad; Hercules, CA). Lysates were mixed with the reducing sample buffer for electrophoresis and subsequently transferred onto nitrocellulose (Bio-Rad) for all blots except for p16, KLF-2, p-ACC and ACC (PVDF membranes, Thermo Scientific). Equal loading was checked using Ponceau red solution. Membranes were incubated with primary antibodies (SI Appendix, Table S2). After secondary antibody incubation (anti-goat, anti-rabbit, anti-rat or anti-mouse, Amersham, GE Healthcare, UK 1/3000), immunodetection was performed using an enhanced chemiluminescence kit (Immun-Star Western C kit, Bio-Rad, or WesternBright™ Sirius,

Advansta for p16 blot) and bands were revealed using the Las-4000 imaging system. After initial immunodetection, membranes were stripped of antibodies and re-probed with anti-GAPDH, anti-actin or anti anti-tubulin antibodies (SI Appendix, Table S2). Values reported from Western blots were obtained by band density analysis using Image Gauge software (Fujifilm, Tokyo, Japan) and expressed as the ratio protein of interest compared to GAPDH, actin or tubulin expression for whole cell extract.

Statistical analysis.

Data are expressed as mean ± SEM for *in vitro* experiments and as median (interquartile range) for *in vivo* experiments. Comparisons between different SS conditions or between control and treatment conditions were performed using a Wilcoxon test. Comparisons between groups of mice were performed using the Mann-Whitney U-test. Comparison between genders was performed using a Chi-square test. Statistical analyses and Figures were performed using the SPSS statistical package 20.0 software for Windows (SPSS Inc., Chicago, IL, United States) and GraphPad Prism 5 software, respectively. All tests were two-sided and used a significance level of 0.05.

Data sharing.

The data that support the findings of this study are available from the corresponding author on reasonable request.

References :

1. Tricot O*, et al.* (2000) Relation between endothelial cell apoptosis and blood flow direction in human atherosclerotic plaques. *Circulation* 101(21):2450-2453.

2. Choi G*, et al.* (2015) Coronary Artery Axial Plaque Stress and its Relationship With Lesion Geometry: Application of Computational Fluid Dynamics to Coronary CT Angiography. (Translated from eng) *JACC Cardiovasc Imaging* 8(10):1156-1166 (in eng).
3. Ramkhelawon B*, et al.* (2009) Shear stress regulates angiotensin type 1 receptor expression in endothelial cells. *Circ Res* 105(9):869-875.

4. Eskelinen EL (2005) Maturation of autophagic vacuoles in Mammalian cells. *Autophagy* 1(1):1-10.

5. Eng KE, Panas MD, Karlsson Hedestam GB, & McInerney GM (2010) A novel quantitative flow cytometry-based assay for autophagy. *Autophagy* 6(5):634-641.

6. Oberlin E*, et al.* (2010) VE-cadherin expression allows identification of a new class of hematopoietic stem cells within human embryonic liver. *Blood* 116(22):4444-4455.
7. Hara T*, et al.* (2006) Suppression of basal autophagy in neural cells causes neurodegenerative disease in mice. *Nature* 441(7095):885-889.
8. Komatsu M*, et al.* (2005) Impairment of starvation-induced and constitutive autophagy in Atg7-deficient mice. *J Cell Biol* 169(3):425-434
9. Warboys CM*, et al.* (2014) Disturbed flow promotes endothelial senescence via a p53-dependent pathway. (Translated from eng) *Arterioscler Thromb Vasc Biol* 34(5):985-995 (in eng).
10. Wang CY*, et al.* (2009) Obesity increases vascular senescence and susceptibility to ischemic injury through chronic activation of Akt and mTOR. *Sci Signal* 2(62):ra11.
11. Jorgensen SB*, et al.* (2004) Knockout of the alpha2 but not alpha1 5'-AMP-activated protein kinase isoform abolishes 5-aminoimidazole-4-carboxamide-1-beta-4-ribofuranosidebut not contraction-induced glucose uptake in skeletal muscle. (Translated from eng) *J Biol Chem* 279(2):1070-1079 (in eng).
12. Duncan GS*, et al.* (1999) Genetic evidence for functional redundancy of Platelet/Endothelial cell adhesion molecule-1 (PECAM-1): CD31-deficient mice reveal PECAM-1-dependent and PECAM-1-independent functions. *J Immunol* 162(5):3022-3030.
13. Orhon I*, et al.* (2016) Primary-cilium-dependent autophagy controls epithelial cell volume in response to fluid flow. (Translated from eng) *Nat Cell Biol* 18(6):657-667 (in eng).

Age (yrs)	79 (72-85)
Male gender	4 (80)
Symptomatic plaques	2 (40)
Stroke	1 (20)
Amourosis	1 (20)
Cardio-vascular risk factors	
Diabetes	2 (40)
Hypertension	3 (60)
Smoking	1 (20)
Dyslipidemia	4 (80)
Body mass index (kg/m²)	28.7 (21.9-35.3)
Treatments	
Antiplatelet therapy	5 (100)
Statins	4 (80)
Beta-blockers	2 (40)
Angiotensin-converting enzyme inhibitors or Angiotensin II receptor antagonist	3 (60)
Calcium channel blockers	1 (20)
Diuretics	2 (40)

Table S1. Patient's characteristics. Data are expressed as median (interquartile range) or frequency (%) (n = 5).

Antibody anti-	Raised in	Reference		Dilution	WB Buffer	IF buffer
4EBP1	rabbit	CST	9452	1/1000	TBST milk	-
phospho-4EBP1 (Thr37/46)	rabbit	CST	2855	1/1000	TBST BSA	-
AMPK	rabbit	CST	2795	1/1000	TBST milk	-
phospho-AMPK (Thr172)	rabbit	CST	2535	1/1000	TBST BSA	-
ATG5	rabbit	CST	8540	1/500	TBST milk	-
ATG7	rabbit	CST	2631	1/1000	TBST milk	-
BECLIN1	rabbit	CST	3495	1/1000	TBST milk	-
CD144	goat	Santa Cruz	sc-6458	1/100	-	PBS BSA
CD31	goat	Santa Cruz	sc-1506	1/200	TBST milk	PBS BSA
CD41	rat	BD Pharmingen	563317	1/20		PBS BSA
ICAM1	goat	R&D	AF796	1/1000	TBST milk	-
KLF-2	goat	Novus biological	NB-10-1051	1/500	TBST milk	
KIF3a	rabbit	Abcam	ab11259	1/2000	TBST milk	-
ULK1	rabbit	CST	4773	1/1000	TBST milk	-
phospho-ULK1 (Ser555)	rabbit	CST	5869	1/1000	TBST BSA	-
LAMP2	goat	Santa Cruz	sc-8101	1/1000	TBST milk	PBS BSA
LC3B	rabbit	CST	2775	1/1000	TBST milk	PBS BSA
p16	mouse	BD Pharmingen	51-1325GR	1/1000	TBST milk	-
p16	mouse	Abcam	Ab54210	1/1000		PBS BSA
GAPDH	mouse	Millipore	mab-374	1/20000	TBST milk	-
TUBULIN	rat	Abcam	Ab6160	1/5000	TBST milk	
ACTIN	goat	Santa Cruz	sc-1616	1/10000	TBST milk	-
p53	mouse	CST	2524	1/1000		PBS BSA
p-ACC	rabbit	CST	3661	1/1000	TBST milk	-
ACC	rabbit	CST	3662	1/1000	TBST milk	-

Table S2. List of antibodies used for western blot analyses. Abbreviations: BSA, Bovine Serum Albumin; CST, Cell Signaling Technologies; IF, Immunofluorescence; PBS, Phosphate Buffer Saline; TBST, Tris Buffer Saline 0.05%Tween; WB, Western Blot.

Duration of SS	ATG5/GAPDH			ATG7/GAPDH			Beclin1/GAPDH		
	HSS	LSS	P value	HSS	LSS	P value	HSS	LSS	P value
2 hrs	1.13±0.03	1.15±0.15	1.00	0.85±0.10	0.94±0.10	0.31	2.19±1.17	1.81±0.46	0.84
6 hrs	1.74±0.33	1.20±0.37	0.13	1.05±0.11	0.86±0.19	0.63	1.57±0.52	1.00±0.17	0.19
12 hrs	1.24±0.19	0.94±0.06	0.31	1.06±0.12	0.94±0.19	0.43	0.94±0.17	1.02±0.11	0.31
24 hrs	1.93±0.53	1.60±0.33	0.30	1.06±0.26	0.73±0.16	0.62	1.07±0.09	1.03±0.07	0.73

Table S3. Shear stress does not modulate ATG5, ATG7 or BECLIN1 expression in HUVECs. Western blot analysis of ATG5, ATG7, BECLIN1. Data are normalized to static condition and expressed as mean ± SEM. n= 5 to 7 per time point and per shear stress condition. There was no significant difference between HSS and LSS in any of these parameters.

	***ApoE*$^{-/-}$*; Atg5*$^{flox/flox}$ (n=9)	***ApoE*$^{-/-}$*; Atg5*$^{flox/flox}$*; VE-cadherin-Cre* (n=11)	***P* value**
Metabolic and morphological features			
Body weight (g)	27.4 (24.3 - 34.8)	28.2 (25.8 - 31.4)	0.76
Male gender (%)	5 (55)	5 (45)	0.44
Arterial blood pressure (mm Hg)	79 (74 - 85)	78 (71 - 83)	0.81
Cholesterol (g/L)	8.9 (7.7 - 10.1)	10.0 (7.5 - 11.3)	0.087
Fasting serum glucose (mg/dL)	84 (77 - 109)	111 (102 - 125)	**0.048**
Spleen weight / body weight (%)	0.5 (0.5 - 0.6)	0.5 (0.4 - 0.6)	0.59
Kidney weight / body weight (%)	ND	ND	-
Liver weight / body weight (%)	4.9 (4.7 - 5.2)	5.0 (4.6 - 5.6)	0.49
Heart weight / body weight (%)	0.6 (0.5 - 0.6)	0.5 (0.5 - 0.6)	0.59
Blood cell count			
WBC (x10^3/mm^3)	4.7 (4.0 – 6.4)	5.4 (3.0 – 9.4)	0.66
Lymphocytes (x10^3/mm^3)	2.9 (2.3 – 3.3)	2.6 (2.1 – 4.4)	0.73
Monocytes (x10^3/mm^3)	0.2 (0.1 - 0.3)	0.2 (0.1 - 0.2)	0.45
Granulocytes (x10^3/mm^3)	2.1 (1.1 – 2.8)	2.7 (0.9 – 3.9)	0.40
RBC (x10^3/mm^3)	6.9 (6.2 - 7.7)	7.3 (6.7 - 7.5)	0.80
Hemoglobin (g/dL)	9.8 (8.5 - 10.4)	10.1 (9.4 - 10.3)	0.66
Platelets (x10^3/mm^3)	626 (556 - 964)	656 (560 - 715)	0.88

Table S4. Metabolic features and blood cell count of 23 weeks old *ApoE*$^{-/-}$*; Atg5*$^{flox/flox}$ *vs. ApoE*$^{-/-}$*; Atg5*$^{flox/flox}$*; VE-cadherin-cre* mice fed a Western diet for 10 weeks. Blood cell count was available for 3 mice per group. Data are expressed as median (interquartile range) or number (%) for the gender. There was no significant difference between both groups in any of these parameters except for fasting glucose (p=0.048).

Abbreviations: ND, not determined; RBC, red blood cell; WBC, white blood cell.

	***Atg5*$^{flox/flox}$** **(n=12)**	***Atg5*$^{flox/flox}$*; VE-cadherin-Cre*** **(n=10)**	***P value***
Metabolic and morphological features			
Body weight (g)	22.4 (20.1 - 27.6)	21.5 (19.9 - 25.0)	0.48
Male gender (number)	5 (42)	4 (40)	0.079
Arterial blood pressure (mm Hg)	78 (73 - 82)	78 (75 - 81)	0.74
Cholesterol (g/L)	1.1 (0.9 - 1.4)	1.4 (1.1 - 1.8)	0.93
Fasting serum glucose (mg/dL)	134 (107 - 144)	125 (108 - 162)	0.93
Spleen weight / body weight (%)	0.4 (0.3 - 0.4)	0.4 (0.3 - 0.4)	0.27
Kidney weight / body weight (%)	0.6 (0.5 - 0.6)	0.6 (0.5 - 0.6)	0.80
Liver weight / body weight (%)	4.0 (3.8 - 4.2)	4.2 (3.5 - 4.5)	0.51
Heart weight / body weight (%)	0.6 (0.5 - 0.7)	0.6 (0.6 - 0.7)	0.91
Blood cell count			
WBC (x10^3/mm^3)	4.3 (3.2 - 5.3)	3.8 (2.7 - 4.8)	0.27
Lymphocytes (x10^3/mm^3)	3.4 (2.8 - 5.0)	3.5 (2.7 - 4.4)	0.89
Monocytes (x10^3/mm^3)	0.3 (0.2 - 0.4)	0.2 (0.2 - 0.3)	0.29
Granulocytes (x10^3/mm^3)	0.2 (0.1 - 0.4)	0.2 (0.1 - 0.2)	0.30
RBC (x10^3/mm^3)	7.1 (6.9 - 7.5)	6.9 (6.5 - 7.6)	0.29
Hemoglobin (g/dL)	13.9 (12.8 - 16.8)	14.3 (12.7 - 15.4)	0.93
Platelets (x10^3/mm^3)	689 (602 - 733)	684 (572 - 787)	0.99

Table S5. Metabolic features and blood cell count of 10 weeks old *Atg5*$^{flox/flox}$ *vs. Atg5*$^{flox/flox}$*; VE-cadherin-Cre* mice fed a chow diet.

Data are expressed as median (interquartile range) or number (%) for the gender. There was no significant difference between the two groups in any of these parameters.

Abbreviations: RBC, red blood cell; WBC, white blood cell.

	***Atg7*$^{flox/flox}$** **(n=12)**	***Atg7*$^{flox/flox}$; *VE-cadherin-Cre*** **(n=10)**	***P value***
Metabolic and morphological features			
Body weight (g)	22.6 (20.2 - 24.1)	21.0 (19.6 - 21.7)	0.27
Male gender (number)	6 (50)	4 (40)	0.46
Arterial blood pressure (mm Hg)	77 (74 - 83)	81 (76 - 84)	0.49
Cholesterol (g/L)	1.5 (1.1 - 1.7)	1.3 (1.1 - 1.6)	0.51
Fasting serum glucose (mg/dL)	150 (139 - 171)	150 (124 - 156)	0.53
Spleen weight / body weight (%)	0.4 (0.3 - 0.5)	0.5 (0.5-0.7)	**0.005**
Kidney weight / body weight (%)	0.6 (0.5 - 0.6)	0.6 (0.6-0.6)	0.55
Liver weight / body weight (%)	5.0 (4.5 - 5.4)	5.1 (5.0-5.3)	0.64
Heart weight / body weight (%)	0.47 (0.45 - 0.49)	0.54 (0.53 - 0.60)	**0.001**
Blood cell count			
WBC (x10^3/mm^3)	3.1 (1.5 - 4.4)	3.3 (2.2 - 3.5)	0.66
Lymphocytes (x10^3/mm^3)	2.8 (1.1 - 3.1)	2.6 (1.8 - 2.7)	0.98
Monocytes (x10^3/mm^3)	0.1 (0.0 - 0.1)	0.1 (0.1 - 0.1)	0.30
Granulocytes (x10^3/mm^3)	0.5 (0.1 - 0.9)	0.6 (0.2 - 1.0)	0.72
RBC (x10^3/mm^3)	6.9 (6.2 - 7.6)	6.1 (5.8 - 6.9)	0.079
Hemoglobin (g/dL)	9.5 (9.1 - 10.6)	9.1 (8.2 - 9.7)	0.18
Platelets (x10^3/mm^3)	657 (456 - 697)	617 (589 - 696)	0.64

Table S6. Metabolic features and blood cell count of 10 weeks old *Atg7*$^{flox/flox}$ *vs.* *Atg7*$^{flox/flox}$*; VE-cadherin-Cre* mice fed a chow diet. Blood cell count was available in *Atg7*$^{flox/flox}$*; and in 9 Atg7*$^{flox/flox}$*; VE-cadherin-Cre mice*.

Data are expressed as median (interquartile range) or number (%) for the gender

Abbreviations: RBC, red blood cell; WBC, white blood cell.

	***Atg5*$^{flox/flox}$** **(n=7)**	***Atg5*$^{flox/flox}$*; VE-cadherin-Cre*** **(n=10)**	***P value***
Metabolic and morphological features			
Body weight (g)	47.1 (43.5 - 52.9)	44.2 (41.8 - 50.7)	0.49
Male gender (%)	7 (100)	10 (100)	-
Cholesterol (g/L)	2.3 (1.8 - 2.9)	3.0 (2.2 - 3.4)	0.19
Fasting serum glucose (mg/dL)	132 (126 - 156)	134 (129 - 144)	0.65
Liver weight / body weight (%)	6.4 (5.1 - 7.1)	4.4 (3.8 - 5.0)	**0.022**
Heart weight / body weight (%)	0.4 (0.4 - 0.5)	0.4 (0.4 - 0.5)	0.47

Table S7. Metabolic features of 64 weeks old *Atg5*$^{flox/flox}$ *vs. Atg5*$^{flox/flox}$*; VE-cadherin-Cre* mice fed a high fat diet for 16 weeks.

Data are expressed as median (interquartile range) or number (%) for the gender.

	***Atg7*$^{flox/flox}$ (n=14)**	***Atg7*$^{flox/flox}$; *VE-cadherin-Cre* (n=10)**	***P value***
Metabolic and morphological features			
Body weight (g)	54.2 (52.4 - 59.6)	54.1 (52.5 - 56.1)	0.69
Male gender (number)	14 (100)	10 (100)	-
Cholesterol (g/L)	2.5 (1.9 - 3.0)	2.0 (1.8 - 2.5)	0.31
Fasting serum glucose (mg/dL)	191 (171 - 207)	184 (159 - 203)	0.66
Liver weight / body weight (%)	5.3 (4.5 - 6.4)	4.8 (3.7 - 6.0)	0.26
Heart weight / body weight (%)	0.3 (0.3 - 0.3)	0.4 (0.3 - 0.4)	**0.028**

Table S8. Metabolic features of 64 weeks old *Atg7*$^{flox/flox}$ *vs. Atg7*$^{flox/flox}$*; VE-cadherin-Cre* mice fed a high fat diet for 16 weeks. Data are expressed as median (interquartile range) or number (%) for the gender.

Figure S1

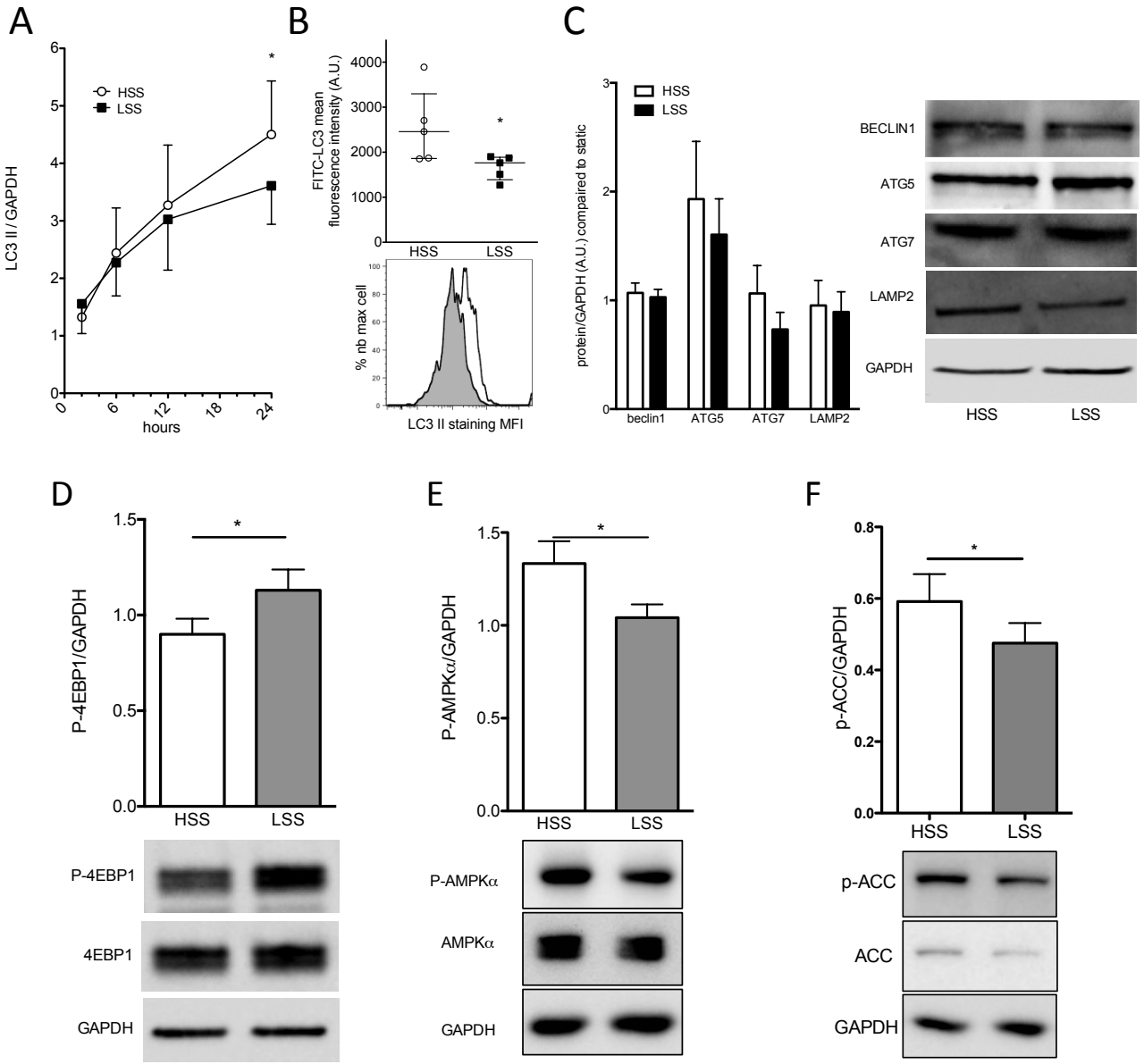

Supplementary Figure 1. Autophagy is defective in endothelial cells exposed to low shear stress. (A) Quantification of LC3 II compared to GAPDH (n ≥ 5 per time point and per condition) in HUVECs exposed to high shear stress (HSS) and low shear stress (LSS). Data are normalized to static condition and are presented as mean ± SEM. (B) Assessment of autophagy level in HUVECs exposed to HSS and LSS for 24 hrs by measuring LC3 staining using flow cytometry (n = 5). Upper panel, quantification; lower panel, representative histogram (gray represents HUVECs exposed to LSS and white HUVECs exposed to HSS). (C) Autophagy related proteins expression in HUVECs exposed for 24 hrs to HSS and LSS (n ≥ 6 per condition). (D-F) 4EBP1, AMPKα and acetyl-CoA carboxylase (ACC) phosphorylations were quantified by western blot in HUVECs exposed to high and low shear stress for 1 (4-EBP1) and 5 min (AMPKα and ACC) (n = 6 for p-4EBP1 and p-AMPKα. n = 9 for p-ACC). *, $p < 0.05$. MFI, mean fluorescent intensity. Figure related to Figures 1 and 3.

Figure S2

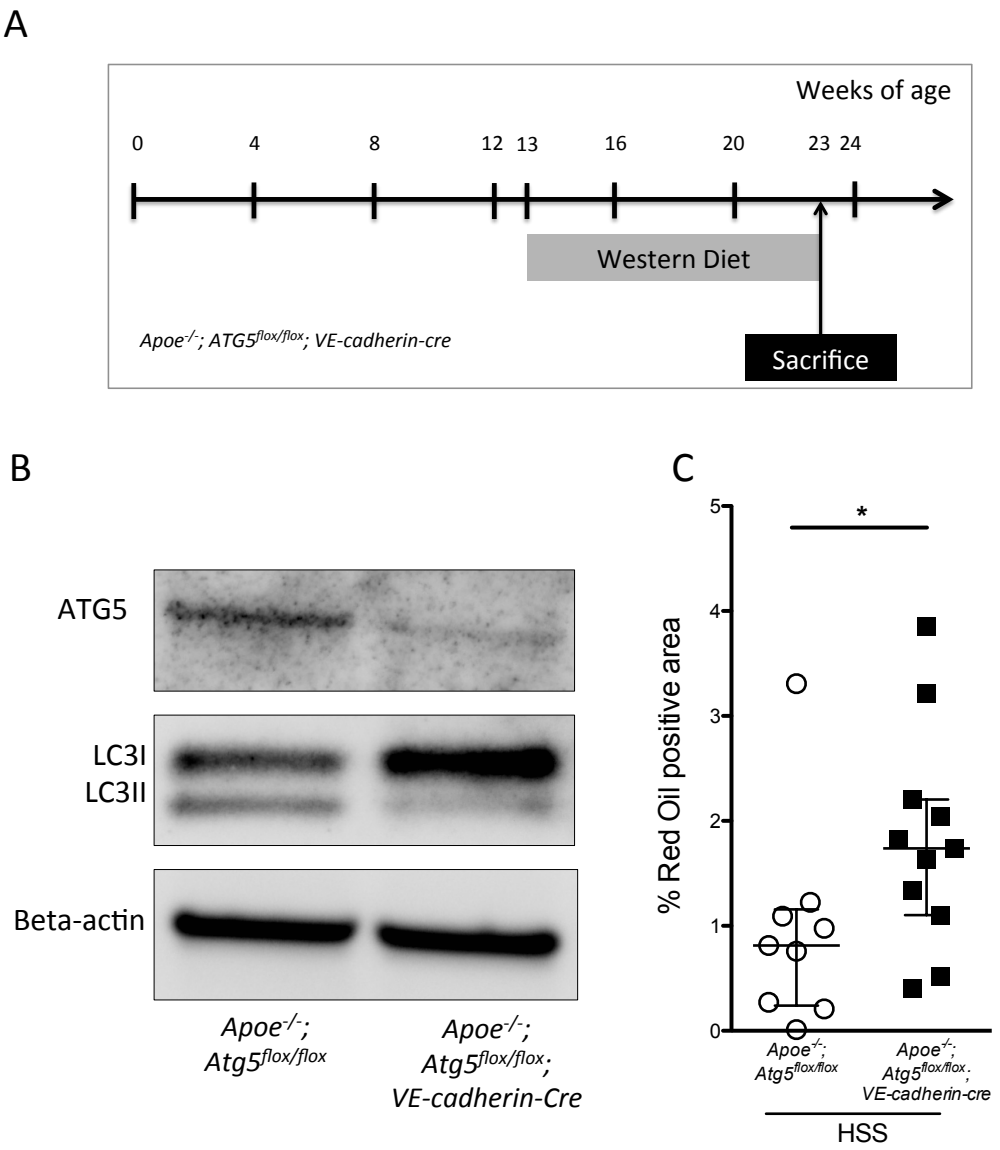

Supplementary Figure 2. *ApoE-/-; Atg5flox/flox; VE-cadherin-Cre* mice are deficient in autophagy in aortic endothelial cells and display increased plaque burden in HSS areas. (A) Protocol to investigate atherosclerosis formation in *Apoe-/-; Atg5flox/flox* and *Apoe-/-; Atg5flox/flox; VE-cadherin-Cre* mice. (B) ATG5 and LC3 levels evaluated by western blot in murine aortic endothelial cells isolated from *Apoe-/-; Atg5flox/flox* and *Apoe-/-; Atg5flox/flox; VE-cadherin-Cre* mice (representative of 2 pools of 4 mice). (C) Quantification of *"en face"* red oil staining of atherosclerotic lesions in the aorta of these mice excluding the ostia of branching points. *, $p < 0.05$. Figure related to Figure 4.

Figure S3

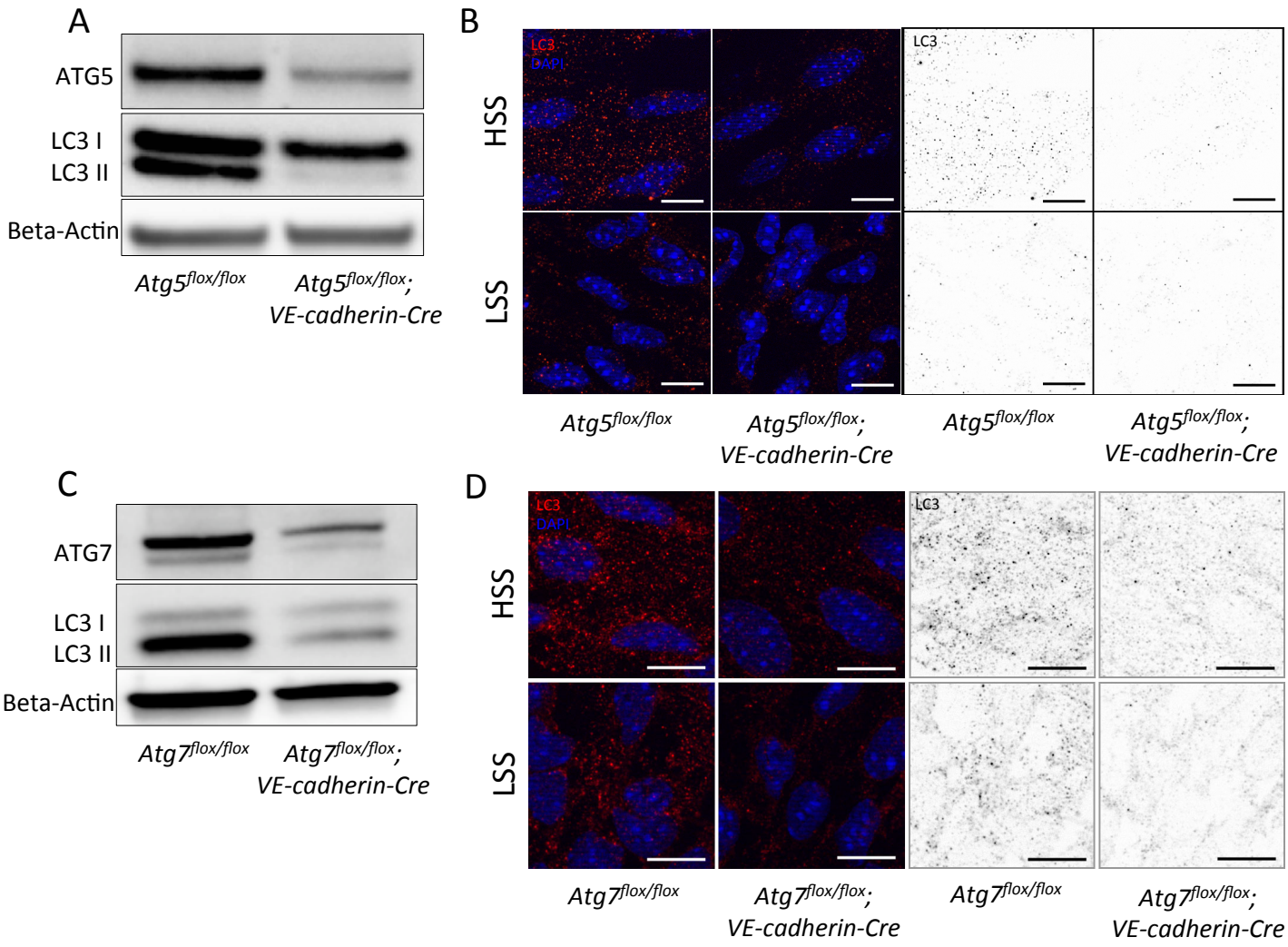

Supplementary Figure 3. *Atg5$^{flox/flox}$; VE-cadherin-Cre and Atg7$^{flox/flox}$; VE-cadherin-Cre* mice are deficient in autophagy in aortic endothelial cells. (A) ATG5 and LC3 levels evaluated by western blot in murine aortic endothelial cells isolated from *Atg5$^{flox/flox}$* and *Atg5$^{flox/flox}$; VE-cadherin-Cre* mice (representative of 2 pools of 4 mice). (B) representative images of LC3 *en face* staining of the aorta of 10 week old *Atg5$^{flox/flox}$ vs. Atg5$^{flox/flox}$; VE-cadherin-Cre* mice (red, LC3; blue, DAPI; n = 5; bar scale, 10 µm; N = 5). (C) ATG7 and LC3 levels evaluated by western blot in murine aortic endothelial cells isolated from *Atg7$^{flox/flox}$* and *Atg7$^{flox/flox}$;VE-cadherin-Cre* mice (representative of 2 pools of 4 mice). (D**)** Representative images of LC3 *en face* staining of the aorta of 10 week old *Atg7$^{flox/flox}$ vs. Atg7$^{flox/flox}$; VE-cadherin-Cre* mice (red, LC3; blue, DAPI; bar scale, 10 µm).-Related to Figure 5.

Figure S4

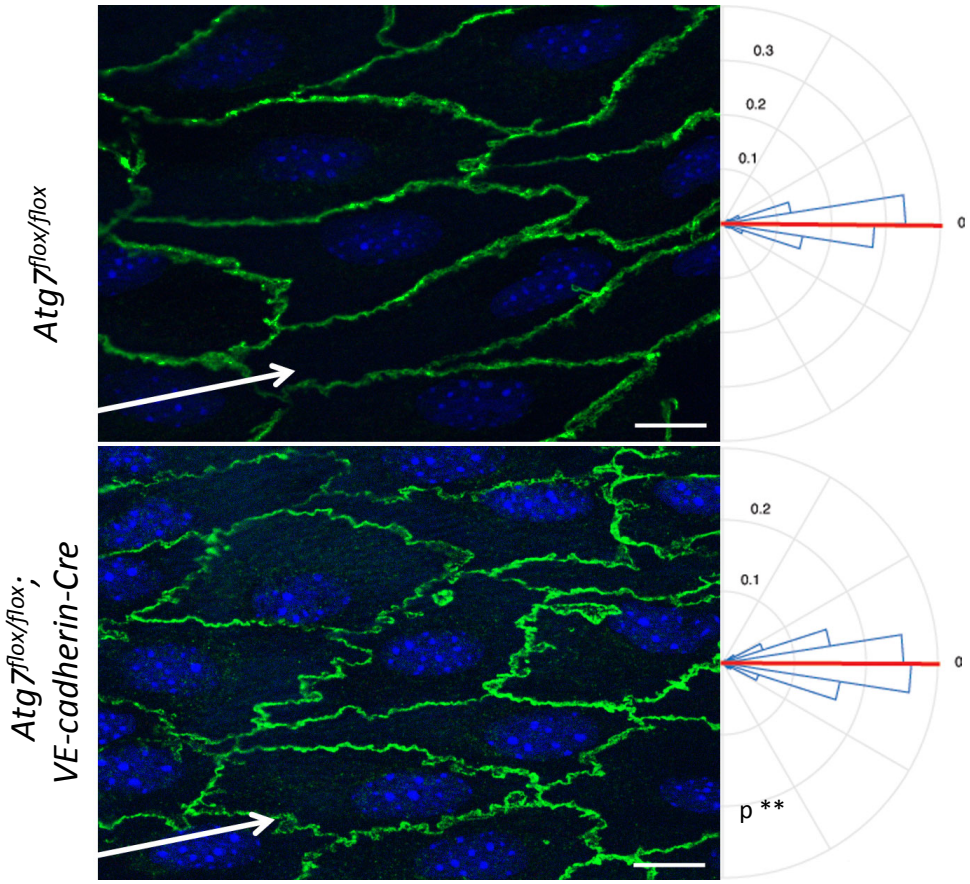

Supplementary Figure 4. Deficiency in endothelial autophagy impairs endothelial cells ability to align in the direction of flow. Quantification of cell alignment in direction of flow in the linear part of the aorta (HSS) of *Atg7*$^{flox/flox}$ or *Atg7*$^{flox/flox}$; *VE-cadherin-Cre* mice (green, CD144 staining; blue, DAPI; n = 5; bar scale 10 μm). **Kp<0.01

figure S5

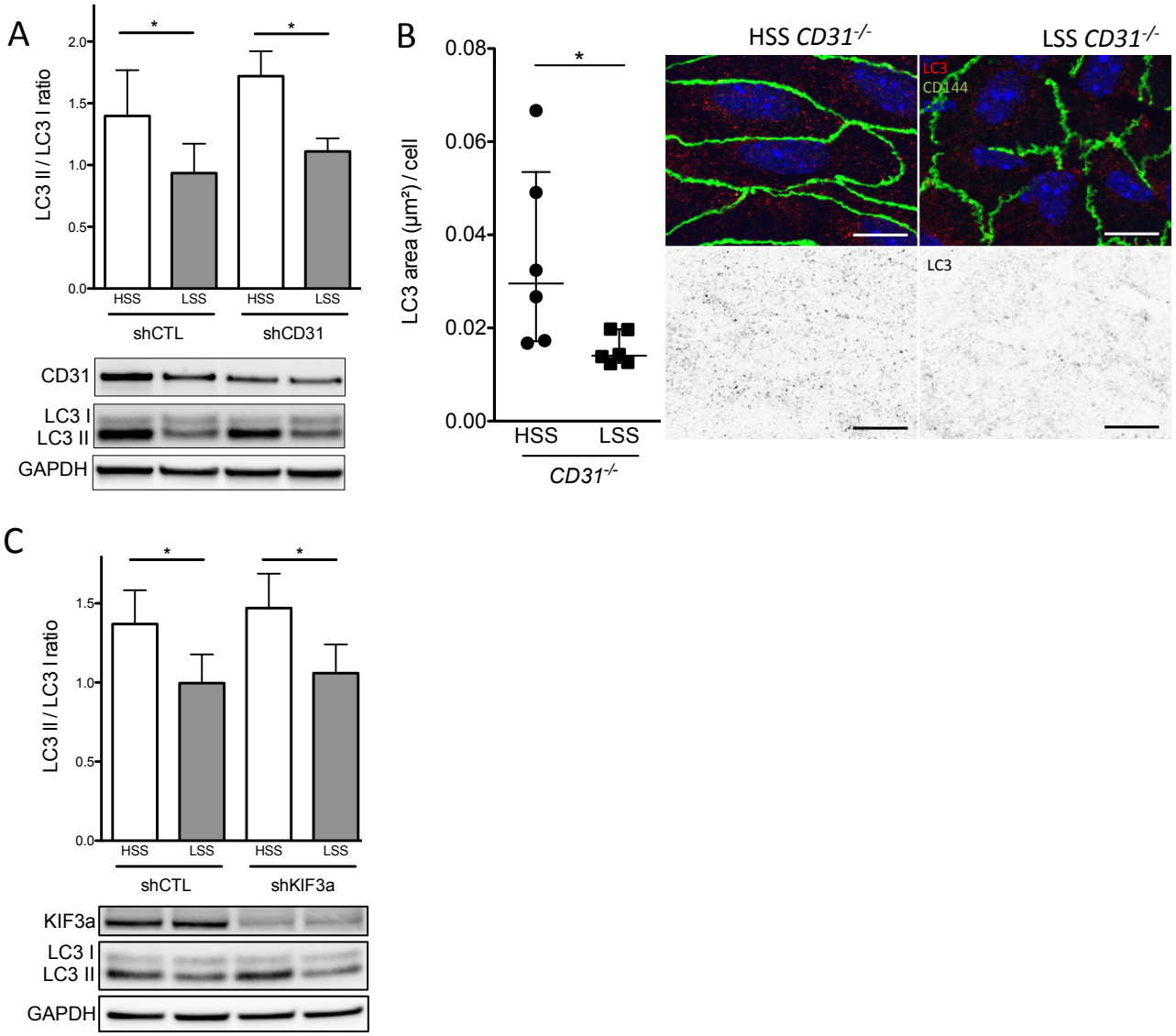

Supplementary Figure 5. The mechanosensor mediating endothelial shear stress effect on autophagy is neither CD31 nor the primary cilium. (A) Western blot analysis of CD31 and LC3 protein expression in HUVECs transduced with a lentivirus expressing CD31 or control shRNA and exposed for 24 hrs to high and low SS (n = 5; shRNA induction: 0.1 mmol/L of IPTG). Data are expressed as mean ± SEM. (B) LC3 *en face* staining of the aorta of 10 week old *CD31-/-* mice (n = 6; green, CD144; red, LC3; blue, DAPI; bar scale, 10 µm). Left, quantification of LC3 area; Data are given as median (horizontal bar) and interquartile range (error bar). Right, representative images. (C) Western blot analysis of KIF3A and LC3 protein expression in HUVECs transduced with a lentivirus expressing KIF3a or control shRNA and exposed for 24 hrs to high and low SS (n = 5, shRNA induction: 1 mmol/L of IPTG). *, $p < 0.05$. HSS, High shear stress; LSS, low shear stress.

Figure S6

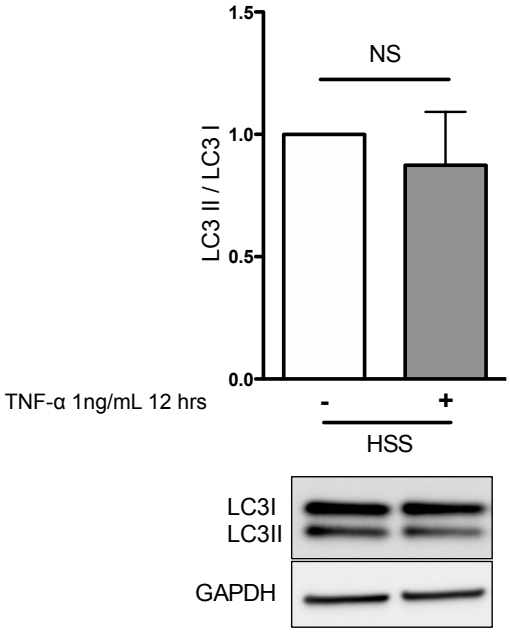

Supplementary Figure 6. TNF-α treatment does not change autophagy level in HUVECs exposed to high shear stress. Western blot analysis of LC3 protein expression in HUVECs exposed for 24 hrs to high SS with or without TNF-α treatment for 12 hrs (n = 6). NS, non significant; HSS, High shear stress.

Figure S7

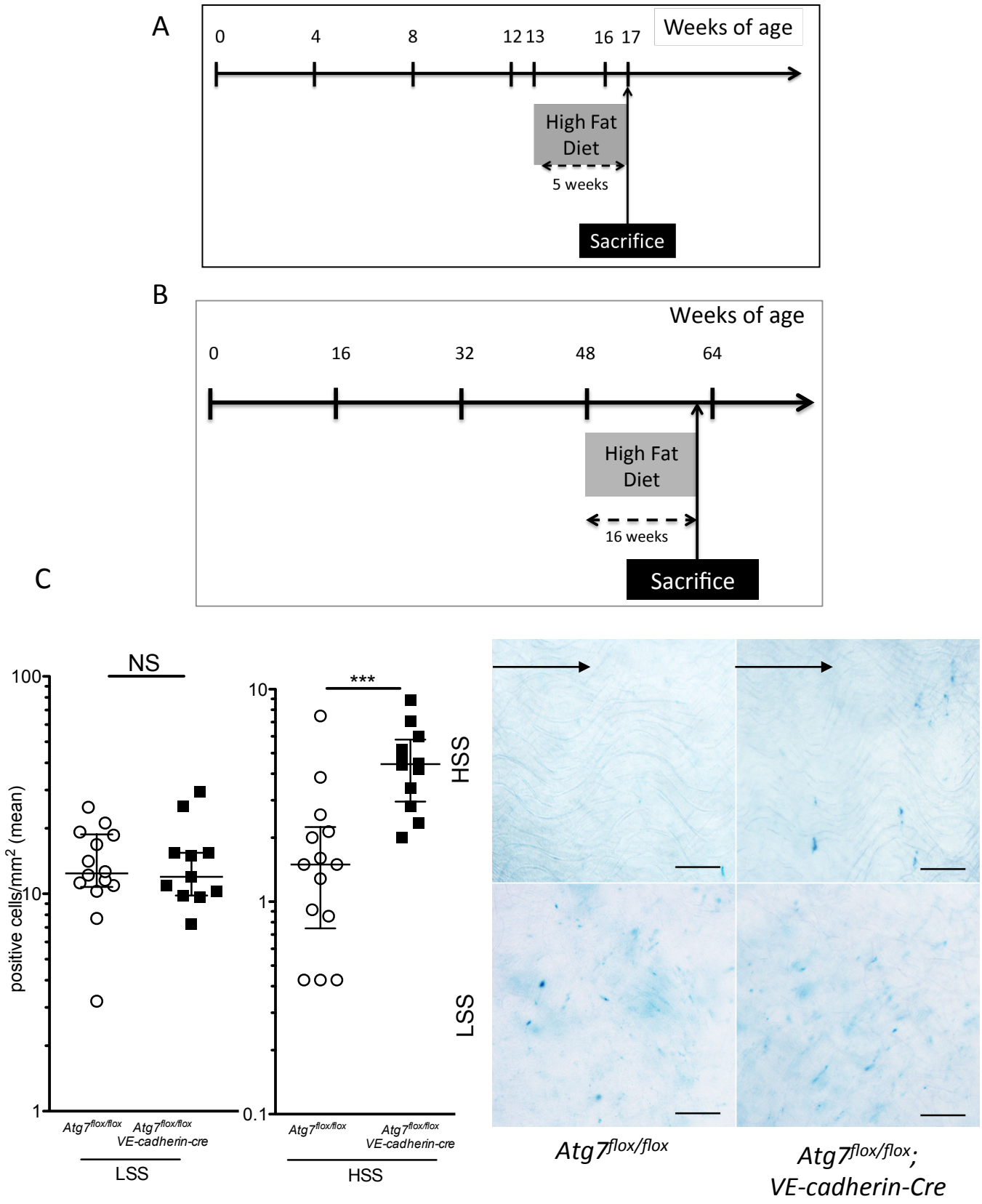

Supplementary Figure 7. Deficiency in endothelial autophagy increases senescence. (A) Protocol to investigate endothelial P53 expression. (B) Protocol to investigate *in vivo* senescence. (C) "*en face*" β-galactosidase staining of the aorta of *Atg7$^{flox/flox}$ vs. Atg7$^{flox/flox}$; VE-cadherin-Cre* mice (n=13 and n=11 respectively). Bar scale, 100 μm; black arrow represents the flow direction. The inner part of the curvature is exposed to SS and the descendant linear part is exposed to high SS. Abbreviations: HSS, High shear stress; LSS, low shear stress. ***, $p < 0.001$ (Mann Whitney test).